No. 8

NUMERICS WAREHOUSE
computer simulations of the natural environment

A Numerical Model Study of the Peak Loads on a Mussel Net Structure During a Storm: – Final Report

By Marcel Curé (Ph.D. Oceanography)
marcel.cure@numericswarehouse.com
www.numericswarehouse.com

30th March 2016

This document is CONFIDENTIAL to the Irish Mussel Seed Company Ltd.

Contract: **A Numerical Model Study of the Peak Loads on a Mussel Net Structure During a Storm: - Interim Report 1**

Customer: Irish Mussel Seed Company Ltd.
22, Church View, Arklow, Co. Wicklow

Recipients: Kate Dempsey

Numerics Warehouse Contract: NW-2016-IRISHMUSSEL-01

Numerics Warehouse Report: NW-2016-IRISHMUSSEL-01_Final_Report

Project Manager: Marcel Curé

Report Revisions

Revision Number	Date	Note	Author
1	03/03/2016	Draft	Marcel Curé
2	15/03/2016	Added mooring design and new bathymetry	Marcel Curé
3	30/03/2016	New net unit and mooring layout	Marcel Curé

Contents

1. Introduction

The aim of this study was to calculate the 50 year storm forces on a mussel farm comprised of flexible net structures which are proposed to be deployed close to Clogga Pt. Co. Wicklow. The location of the proposed mussel farm is bounded by the corners (6.13643 W, 52.75520 N), (6.12755 W, 52.75506 N), (6.12797 W, 52.74518 N) and (6.13685 W, 52.74532 N). All coordinates are WGS84.

The brief was to use this information to design the appropriate net unit layout and anchor system for the net units. The calculations presented here can be used by the mussel farm and anchor manufacturers to specify equipment that best suits this location, assisting with our understanding of the local environment and therefore without having to overspecify the anchors, mooring chains and the net unit components. The results in this report and the accompanying electronic data will also be used in the foreshore license application.

The area around Clogga Pt. is somewhat protected by sand banks and by the adjacent coast from the prevailing winds, so it was unclear at the outset from which direction of wind the mussel farm would be most exposed and what contribution the orbital motion of the waves and tidal currents would have on the force. In addition to calculating the forces on the moorings due to the maximum summertime wind speed that could be expected in a 50 year period, it became quickly apparent that in this study we could also calculate the shape of the nets in response to extreme forces and hence design the nets to best utilise the area of the farm.

This report includes the results from a coupled wave-hydrodynamic numerical model of the Irish Sea and the immediate area around Clogga Pt. The simulations of extreme winds from the directions N, NE, E, SE, S, SW, W and NW were then used to load the mussel laden nets and hence calculate the net shape, the forces and the mooring responses. The calculations can then be used to specify the appropriate anchors, the net unit spacing, the mooring chain size and weight and the mussel headrope characteristics so that they can survive a 50 year storm.

2.0 Methodology

There is no clear guidance yet from standards as to how to calculate the extreme forces on a flexible net structure. BS 6349 'Marine Structures' recommends the application of Morison's equation when a marine structure presents a narrow aspect to waves and currents. We seek to apply some more recent methods which allow the response of the net structure to evolve under a load. Such calculations will be more accurate.

The method used in this study was to numerically model the combined action of waves and 3D currents in the vicinity of the mussel farm. We first calculate the extreme wind speeds that have a Return Period of 50 years from each of the 8 directional sectors, N, NE, E, SE, S, SW, W and NW. The numerical models are forced with a combination of these winds and that spring tide that is theoretically greatest. The outputs from the modelling are a series of 2 and 3D fields, including currents and various wave parameters. From the significant wave height we derive hmax, the 'maximum wave height', and then use simple linear wave theory to calculate the maximum horizontal velocity at the depth of the middle of the nets at each location that there is a net. This instantaneous wave velocity is combined with the modelled spring tidal current at this depth and velocity components are calculated perpendicular to and in line with each net. The currents are assumed 'steady', which is the conservative approach, since there is no accepted theory yet to model the time evolution of the flexible net structure. The perpendicular component is used to calculate the drag and lift on the net at all vertical levels for its steady state shape – a lifted curtain. The net is assigned a weight distribution including bottom weights and either juvenile mussels or pre-harvest mussels (we examine each case). The force at the top of the net, just beneath the sea surface, acts horizontally and perpendicular to the axis of the net. This force is assumed to be uniformly distributed, although once the head rope has deformed substantially, this may no longer be the case. At any rate, this horizontal force will act to both stretch and deform the elastic head rope on the net. This deformation is assumed to be symmetrical, although the combined action including the in-line force will in reality cause the net to 'sag' towards the down current end. Providing the tension in the mooring is great enough this sag should not be substantial. We use a simple elastic rope theory, such as is used for suspension bridge design to calculate the tension in the head rope, its stretch and deformation perpendicular to the net axis.

In this study we have assumed that waves will pass each net 'instantaneously'. This we feel is valid since, as will be shown, the wave crests do not have a big angle with respect to the line of the nets and these long wavelength waves travel very rapidly so that the time difference between a crest passing one end of the net and then passing the other end of the net will be of the order of 1 s. We do not believe that the net structure could respond to such a rapid force change travelling along the net length.

We also calculate the force in the direction of the predominently tidal current. We do this using a simple drag formula for mussel laden net twine, assuming a value of drag coefficient. We have not included any shielding for this, since the net is a 3D structure. The aim of the study was to calculate the total mooring force at the end of each net unit, the tension at the end of each individual net so that they each deform laterally by predominantly the same extent, the extension and deflection of the mooring chain and the forces acting on the anchors. By combining the mooring response with the net unit response we can then examine whether adjacent net units will touch each other under an extreme load, or whether the net units will stay inside of the propesed license area. We also can use the results to ensure that suitably dimensioned components and materials are used for the head ropes of the net units and the anchors and mooring chain under the extreme loads.

3.0 Extreme Wind Analysis

The 6 hourly ERA-Interim wind speed data at 10 m height, from 1979 to 2015 was downloaded from ECMWF. This reanalysis data is widely regarded as being the most accurate generally available gridded dataset for wind. Only data from the summer period (June, July and August) were included in the analysis, since this is when the nets will be loaded with large mussels and the resulting forces will be at their largest. The nearest ERA-Interim grid point to the Clogga site was selected for analysis. This was at 51.75 N, 6.00 W. The data was split into 8 different directional sectors – N, NE, E SE, S, SW, W and NW.

These time series are analysed by applying various wind speed thresholds (Potential Over Threshold, or POT). The peaks that exceed the thresholds are identified and the peak values and the time between them are stored. These are then fitted to the two parameter Weibull distribution. The two parameters are systematically altered until the best fit (in the least squares sense) is found. Typically the regression coefficient is better than 0.99. Once this has been accomplished the tail of the resulting distribution is examined to find out the values of the extreme wind speeds for selected Return Periods. The method depends critically on the value of the POT threshold used. The data here has been generated using a few thresholds to see how sensitive the results are to these and then the most appropriate threshold selected.

The 50 year Return Period (henceforth RP50), wind speeds from each of the 8 sectors were processed using the extreme value algorithm. The results are shown in Table 1.

Table 1 50 Year Return Period Wind Speeds

Wind Direction	RP50 Wind Speed (ms^{-1})
N	18.69
NE	15.21
E	14.17
SE	17.89
S	19.00
SW	19.45
W	18.92
NW	17.04

The data is plotted in figure 1. It can be seen that whereas the strongest wind is from the SW and W, the waves from these directions are not expected to be very large due to the limited fetch. From this data it is not clear from which direction the largest waves are likely to arrive. For this reason, it was decided to run the numerical model with a constant wind with the RP50 value for each of the 8 directions.

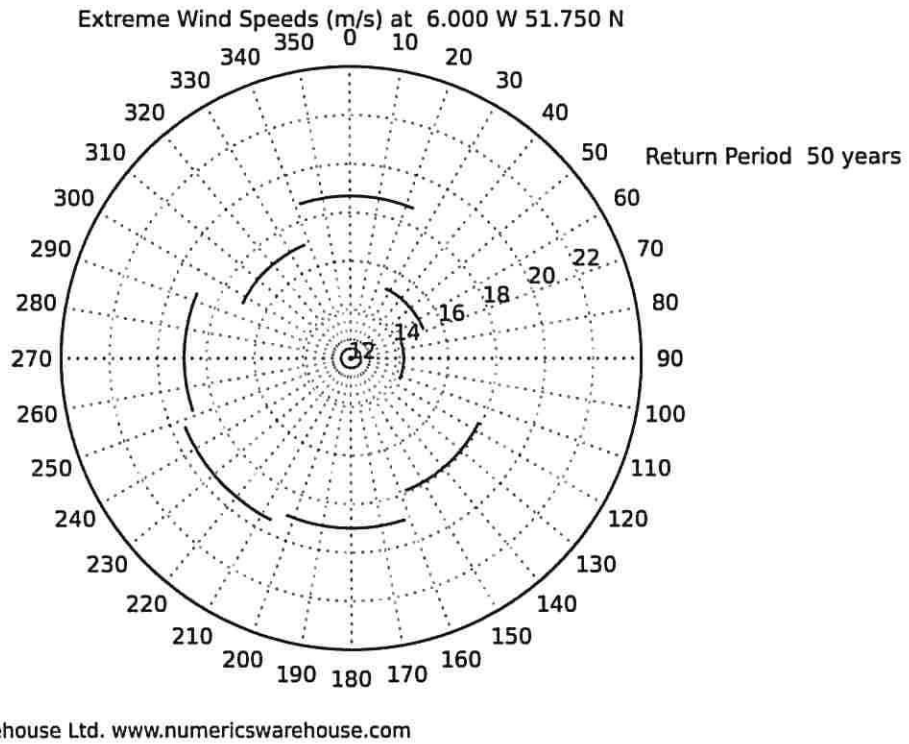

Figure 1. Sector plot showing the 50 year Return Period wind from 8 directional sectors.

4.0 Numerical Modelling

Two separate numerical models have been developed as part of this project. The first covers the entire Irish Sea at a resolution of 1 km and with 20 vertical layers. The purpose of this model was to properly simulate the complex tides in the Irish Sea in order to provide boundary conditions to a high resolution model around Clogga Pt, where the proposed Mussel farm will reside. The high resolution model has a grid size of approximately 100 m. The other reason to cover such a large area was to include an adequate fetch for the wind wave generation in the numerical model. The two models are called COAWST_Isea and COAWST_Clogga and their extents and resolution are shown in Table 2.

Table 2

Model Name	Extent Lat.	Extent Lon.	Resolution	Comment
COAWST_ISea	51.90 to 55.20	-6.65 to -2.60	0.015 by 0.010	nx = 271, ny = 331 20 vertical levels
COAWST_Clogga	52.650 to 52.850	-6.252 to -6.000	0.0015 by 0.0010	nx = 169, ny = 201 20 vertical levels

Both COAWST_Isea and COAWST_Clogga are coupled wave-hydrodynamic models. They use the modelling system COAWST, which represents the state of the art in ocean modelling. COAWST (http://woodshole.er.usgs.gov/operations/modeling/COAWST/) couples the 3D hydrodynamic model ROMS (http://www.myroms.org) with the spectral wave model SWAN (http://www.swan.tudelft.nl/). In the implementation here, SWAN and ROMS both share the same horizontal grid. They were both run on separate parts of a supercomputer (HPC) concurrently and periodically shared data between the models. In this way the waves were generated on top of the 3D model solution and were affected by the changing tide and the currents in a realistic way. Conversely the waves themselves generate currents (Stokes drift) and turbulence which are added to the hydrodynamic currents.

The spectral wave boundary data for COAWST_Isea was generated by an ocean scale wave model WaveWatch3 (http://polar.ncep.noaa.gov/waves/index2.shtml). This model was run as part of this project with a domain covering the entire North Atlantic basin. In this way those swell waves which have traversed the Atlantic are accurately included in the simulations here.

The FORTRAN based models were run on an in house Linux based High Performance Computer in Numerics Warehouse Ltd.

4.1 Model Bathymetries

One of the biggest tasks in this project was to source some good bathymetry to describe the model sea beds. The highest quality data was to be found from a survey of the prospective license area by Geo-Mara Ltd. and the national agency INFOMAR (www.infomar.ie) who have conducted some high resolution swath multibeam acoustic surveys in the area. These were the preferred data sources, but did not cover the area close to the coast. The UK Admiralty charts 1787 and 1468 were digitised and used as a secondary source of data. To the LAT depths was added the Mean Tide level determined from a 19 year tide record derived from the global tide model TPXO 7.3. The final source of data used was GEBCO (www.gebco.net). The coastline was defined using both the USGS

GEODAS adtaset and the digitised Admiralty coastline. The resulting bathymetries and their sources of data are shown in figs. 2-5.

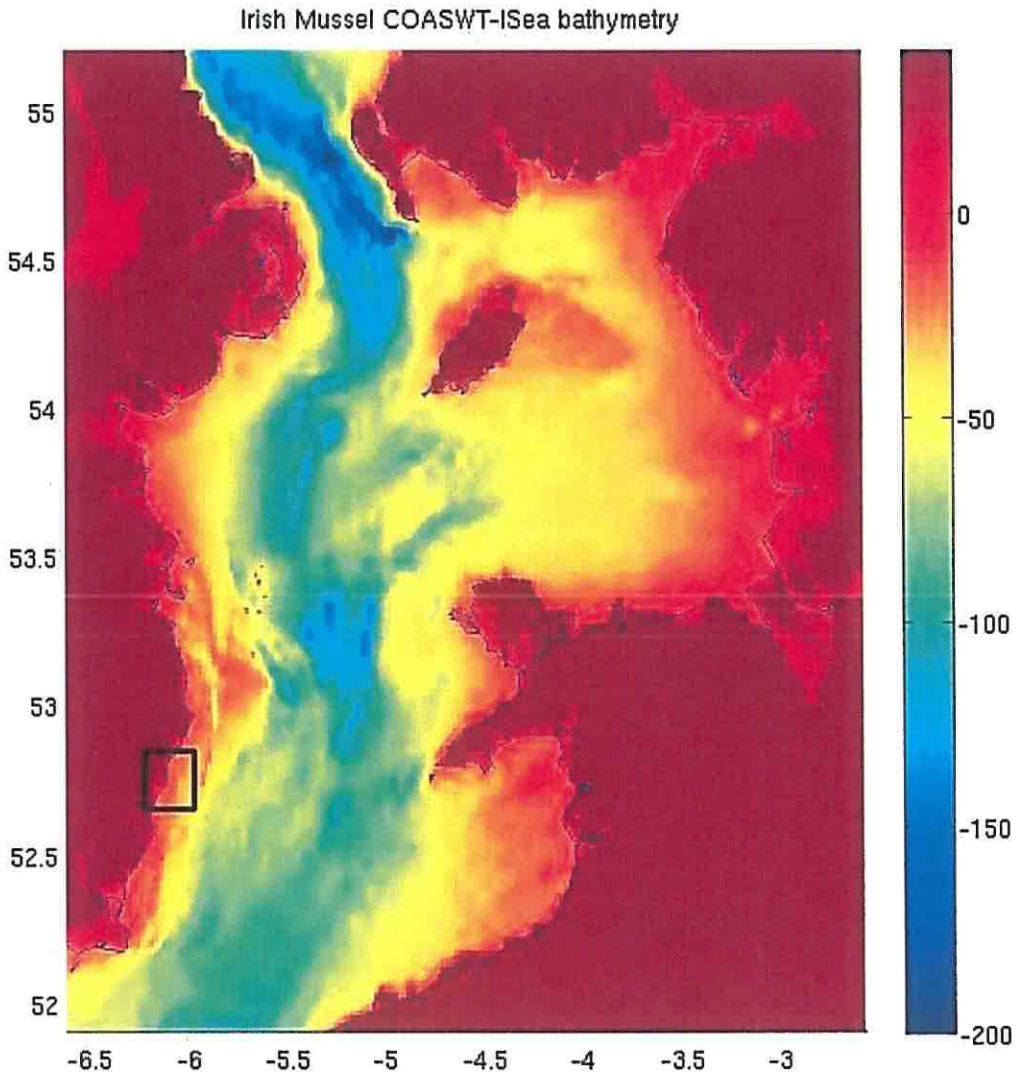

Figure 2. Bathymetry of the model COAWST_Isea. The black box shows the boundary of the high resolution model COAWST_Clogga.

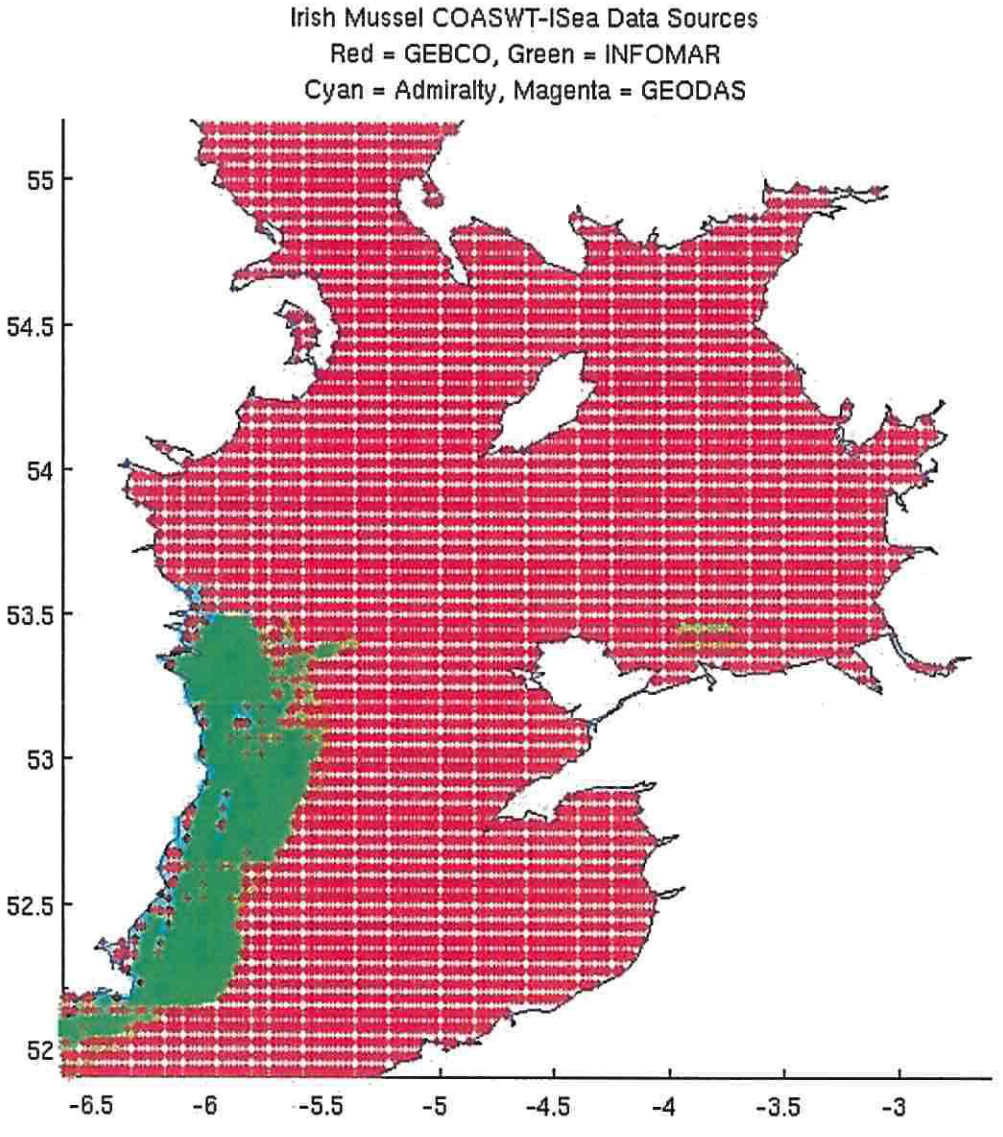

Figure 3. Sources of data for the model bathymetry of COAWST_Isea.

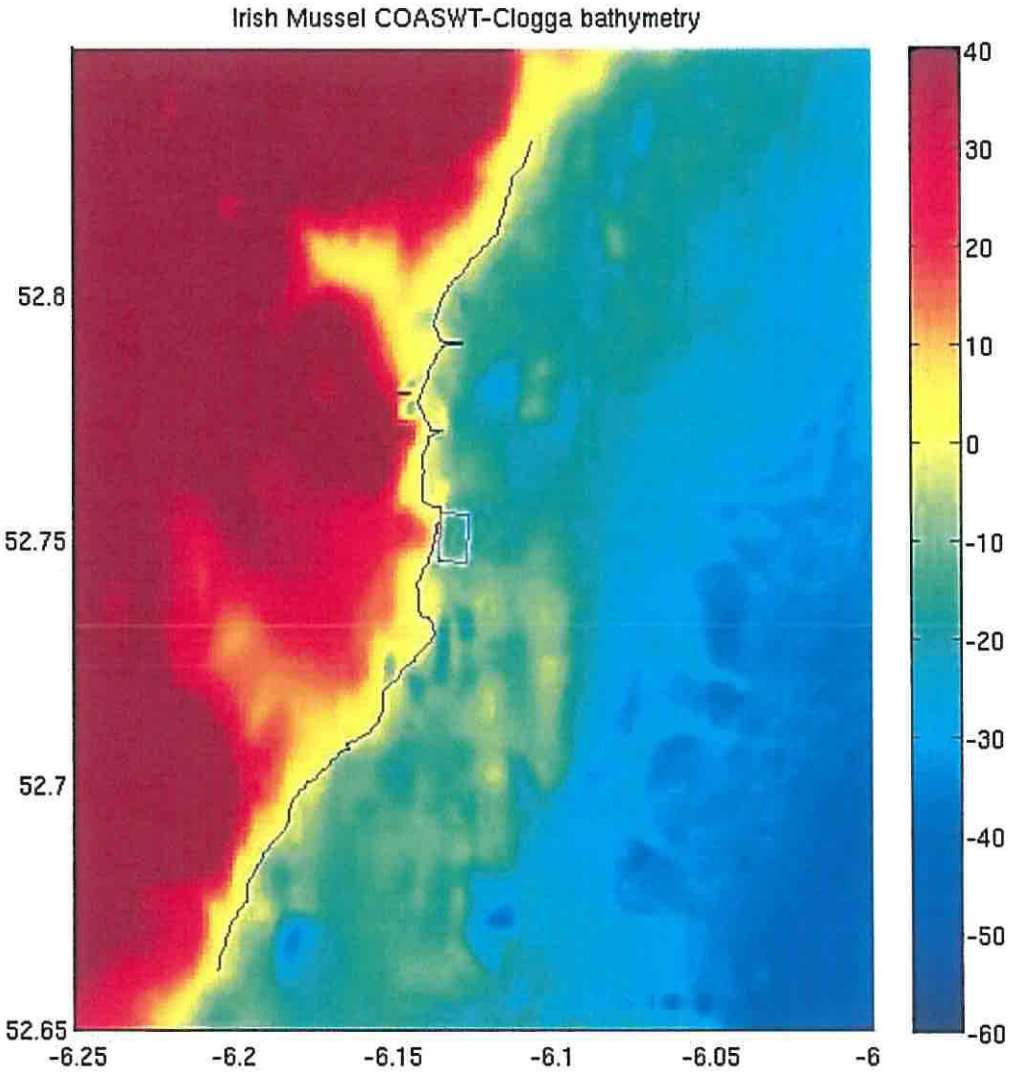

Figure 4. Bathymetry for the model COAWST_Clogga, also showing the license area as a magenta rectangle.

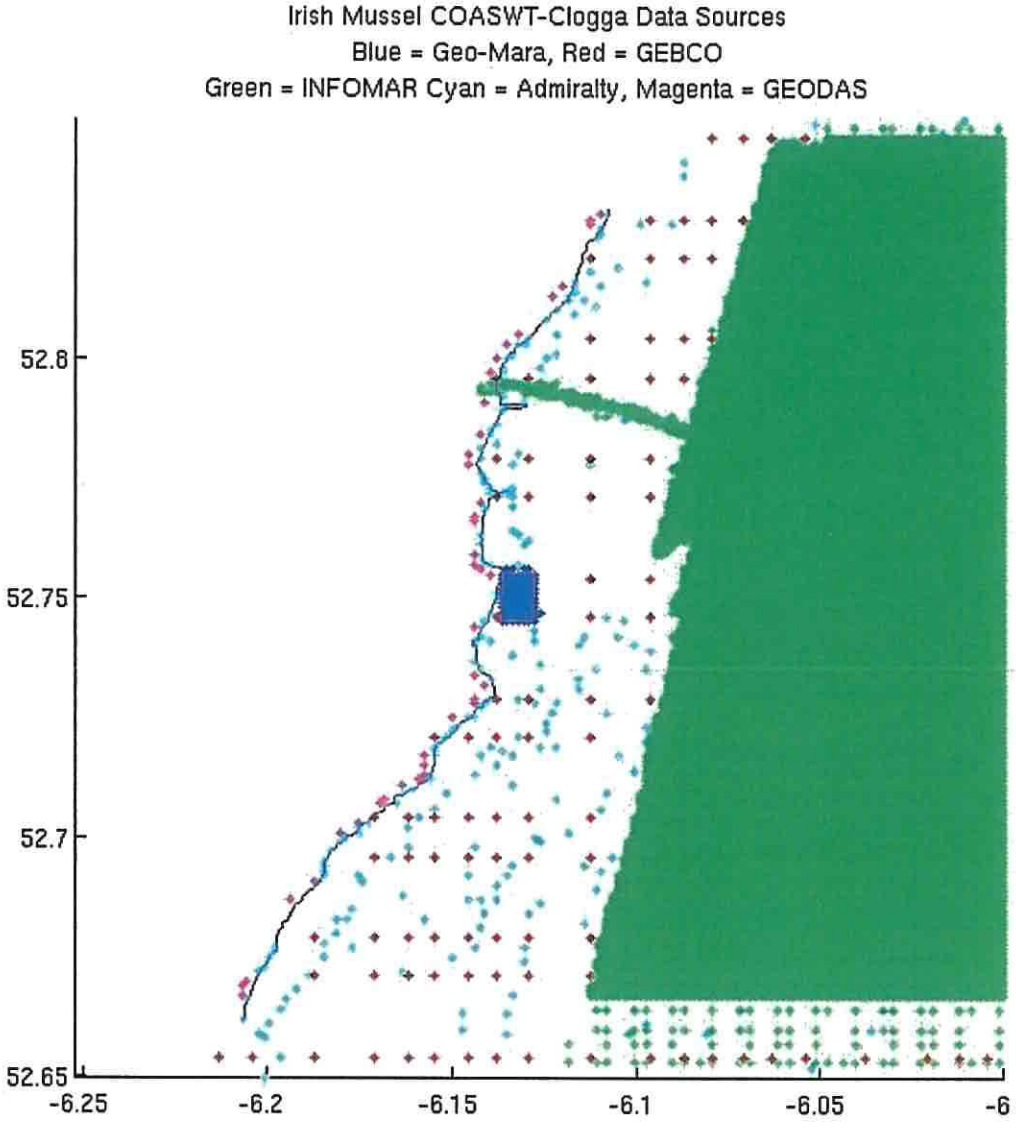

Figure 5. Sources of data for the model bathymetry of COAWST_Clogga.

4.2 Model Forcing, Boundary and Initial Conditions

The model COAWST_Isea was prescribed climatological boundary and initial conditons corresponding to the World Ocean Atlas 2009. The 12 tidal constituents from the global tidal HYCOM model TPXO 7.3 of the Oregon State University, with its assimilated satellite altimeter data was used. The 3D currents, temperature, salinity and sea levels were fed into the nested COAWST_Clogga.

Both of the models were forced with wind speed, direction, air temperature, solar and longwave radiation, precipitation and humidity derived from ECMWF ERA-Interim.

4.3 Model Station Output

The area around the proposed Clogga mussel farm is shown in figure 6.

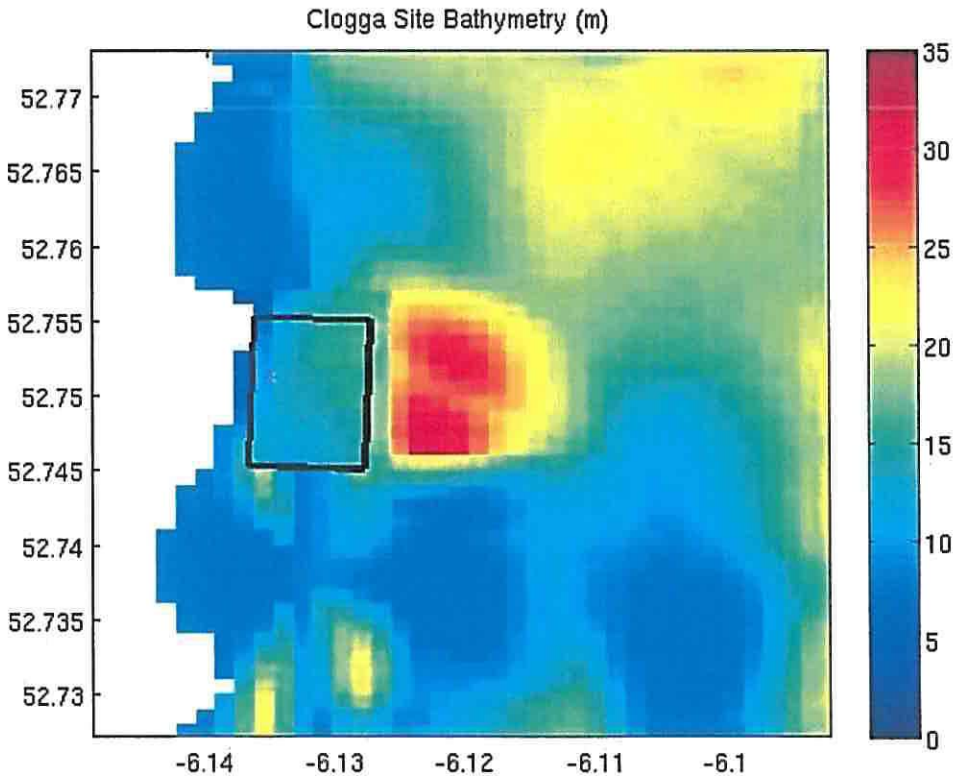

Figure 6. Bathymetry around the limits of the Clogga mussel farm, shown as a black box. The position of the AquaDopp acoustic current meter used in validation of the model is shown as a magenta cross.

Five stations were selected to output high temporal resolution model data from. These were at the position of an AquaDopp current meter used to collect the data and used here to validate the model, as well as the four corners of the site. For these locations, model output was collected every 10 minutes. The data collected includes 3D currents, temperature and salinity, sea surface height, significant wave height, mean wave period, mean wave direction and peak wave period. The station numbers and their positions are

shown in table 3.

Table 3

Station Number	Latitude	Longitude	Comment
1	52.75129 N	-6.13528 W	AquaDopp meter
2	52.75520 N	-6.13600 W	NW corner
3	52.75506 N	-6.12755 W	NE corner
4	52.74518 N	-6.12797 W	SE corner
5	52.74532 N	-6.13685 W	SW corner

4.4 Determination of the Largest Tide at Clogga Pt.

We wish to find the most extreme tide (and hence forcing on the mussel nets) that can occur at the farm location.

The tide is subject to a nodal cycle (caused by the precession of the moon's orbit with respect to the Earth) of duration 18.6 years. For this reason it is necessary to examine this duration to find the most extreme astronomical tide in the area. By extracting tidal heights from the global tidal model TPXO 7.3, it was determined that this occurred in the few days at the end of January 1993. The models were run starting before this date to allow model spin up. The largest south flowing tidal current occurred at 1993/01/26 1600 and the largest north flowing tide occured at 1993/01/26 2130.

5.0 Model Validation and Errors

The COAWST_Clogga numerical model was run for the period 14/06/2015 to 30/07/2015, allowing for the model spin-up and coincident with the AquaDopp acoustic sounder deployed at location 52.75129 N, 6.13528 W. The AquaDopp data was extremely noisy, with many invalid records. These were removed by setting a threshold of 3.0 ms^{-1} and deleting any records exceeding this level. The model solution (Station 1 of the model output) was interpolated to three depths corresponding to the near bottom, mid depth and near surface time series of the AquaDopp and then compared. Figure 7 shows the velocity magnitude at the 3 depths for the duration of the acoustic data.

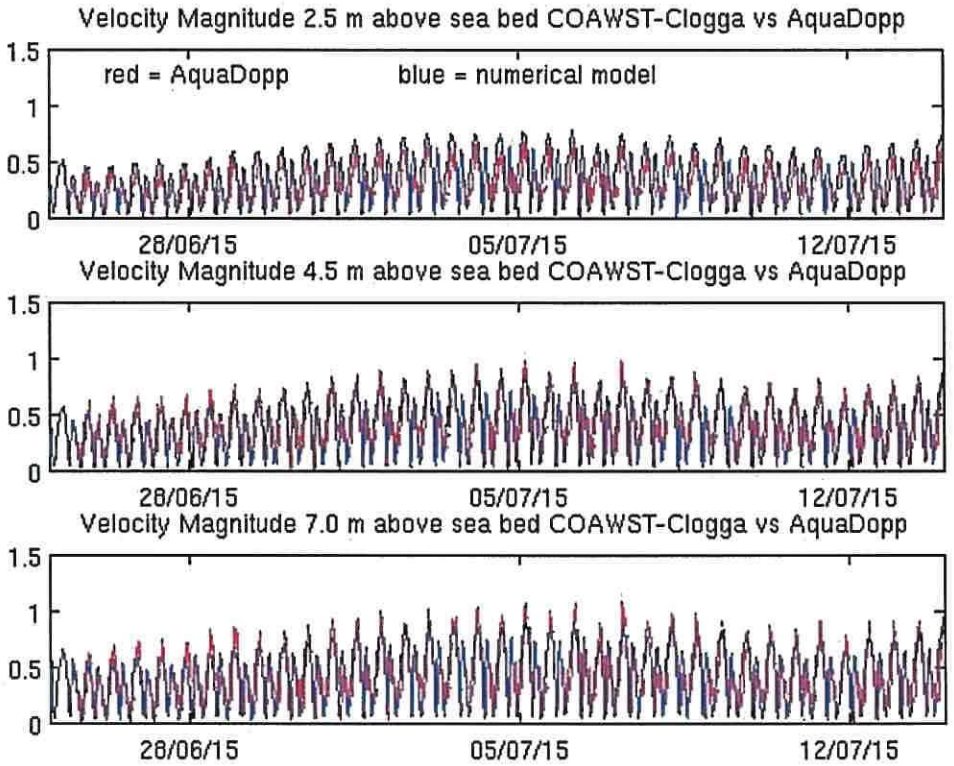

Figure 7. Comparison of model solution for velocity magnitude with AquaDopp at three vertical levels.

The model current direction is plotted against the AquaDopp for the mid depth position (it does not vary much with depth) in figure 8. Finally a blow up of a few days is shown in figure 9 for velocity magnitude at mid depth.

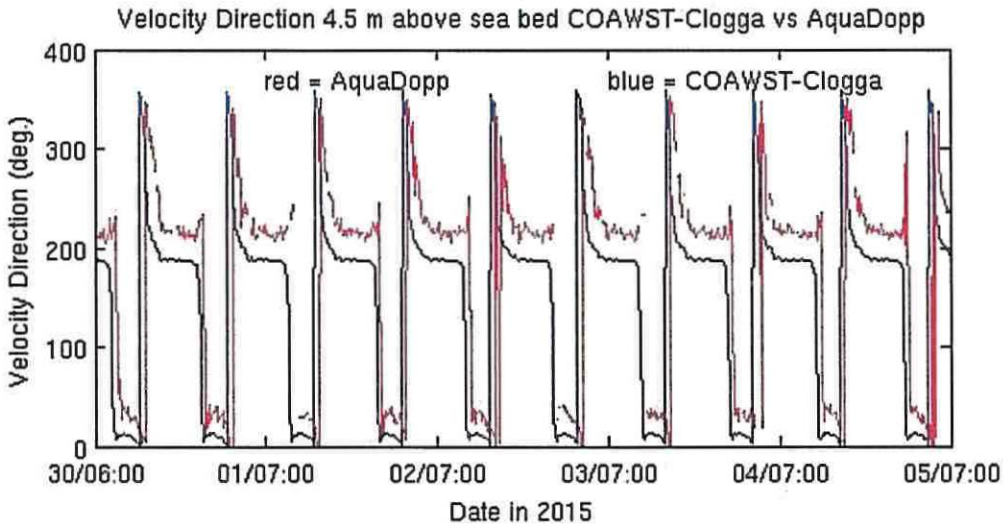

Figure 8. Comparison of model solution for velocity direction with AquaDopp at mid water depth.

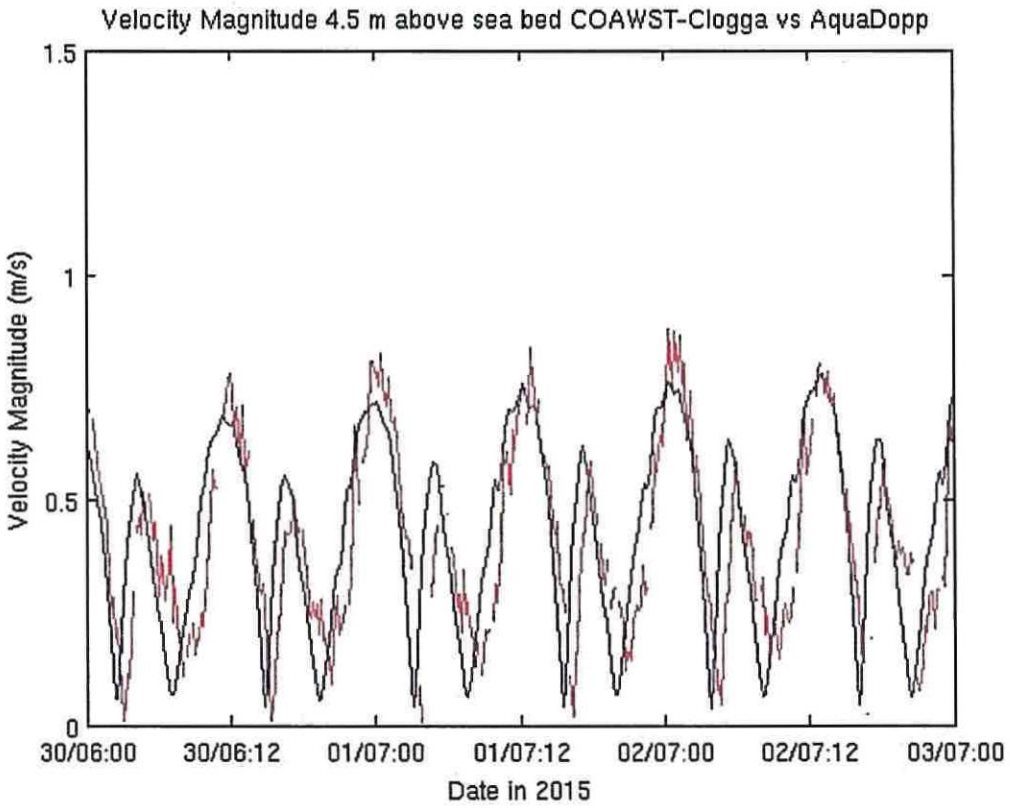

Figure 9. A blowup of the velocity magnitude data for 5 days at mid depth.

The model solution demonstrates that it is quite good when compared to the acoustic current meter data. It reproduces the spring-neap cycle, it shows a good variation of the velocity magnitude with depth, with peak values of 0.6 ms^{-1} close to the sea bed and 1.0 ms^{-1} close to the surface. The model solution underpredicts the acoustic data by approximately 0.1 ms^{-1} at peak flood and ebb flows close to the sea surface. The model reproduces the assymmetry between the 2 principle semi-diurnal tides. The velocity direction comparison is not as good, with errors of approximately 20 degrees. This is likely due to some errors in the local bathymetry around the AquaDopp. The data from the Admiralty chart is about 2 m shallower than the depth record from the current meter. The directional error is not thought to be very important, since when taking direction cosines, this will introduce a velocity error of only 6% and the tidal currents are not nearly as large as the instantaneous wave orbital velocity as will be shown later.

In conclusion, the newly developed COAWST_Clogga model solution is considered suitable for analysis of the ocean response to extreme wind simulations.

6.0 Extreme Wind Model Solutions

The combined model solution was run in turn with RP50 steady winds from each of the 8 directions N, NE, E, SE, S, SW, W and NW. The largest tides of January 1993 were included to arrive at the most severe set of conditions that can be foreseen. For each of the cases, the waves had reached a quasi-steady state significant wave height within 48 hours. We can conclude that a storm which maintains a steady wind speed and direction for this duration, as it sometimes does, will not be surpassed in terms of the instantaneous wave particle orbital velocity at the Clogga site.

Figure 10 shows the significant wave height reached with the wind from each of the sectors in the COAWST_Isea model solution. It can be seen that winds from the north, north east, south east and south all produce high waves in the proposed mussel farm area.

In all wind direction cases except west and north west , it is found that the waves are refracted to head more towards the shore as they feel the bottom. This can lead to waves and wind having very different directions at the mussel farm site. Table 4 shows the significant wave height, direction and peak wave period for each of the wind directions for station 3 at the NW corner of the site extracted from the COAWST_Clogga model.

Table 4

Wind Direction	Sig. Wave Height (m)	Peak Wave Direction (from Deg.)	Peak Wave Period (s)
N	2.67	037	8.56
NE	2.64	025	7.54
E	2.47	090	7.03
SE	3.15	115	8.35
S	2.82	134	10.88
SW	1.92	115	13.48
W	1.35	115	13.87
NW	1.32	241	7.61

Before the commencement of this study and following discussions with Irish Seed Mussel Company Ltd., it was thought that the most severe waves would result from a north wind. The results of the modelling, however indicate that the highest waves occur when the wind is from the south east, even though the RP50 wind speed is not particularly high. The high waves resulting from the south wind were not expected, since there is a shallower area to the south of the site. This submerged bank does indeed reduce the waves, but since the RP50 wind speed is very high and also since these long period swell waves are steered into the region, originating in the Celtic Sea, there remains a considerable wave energy at the site.

The waves generated by the RP50 winds from the south, south west and west are all swell, or long period waves, not generated within the Irish Sea. Their presence vindicates the modelling approach adopted here of nesting the wave model into the North Atlantic WaveWatch 3 model.

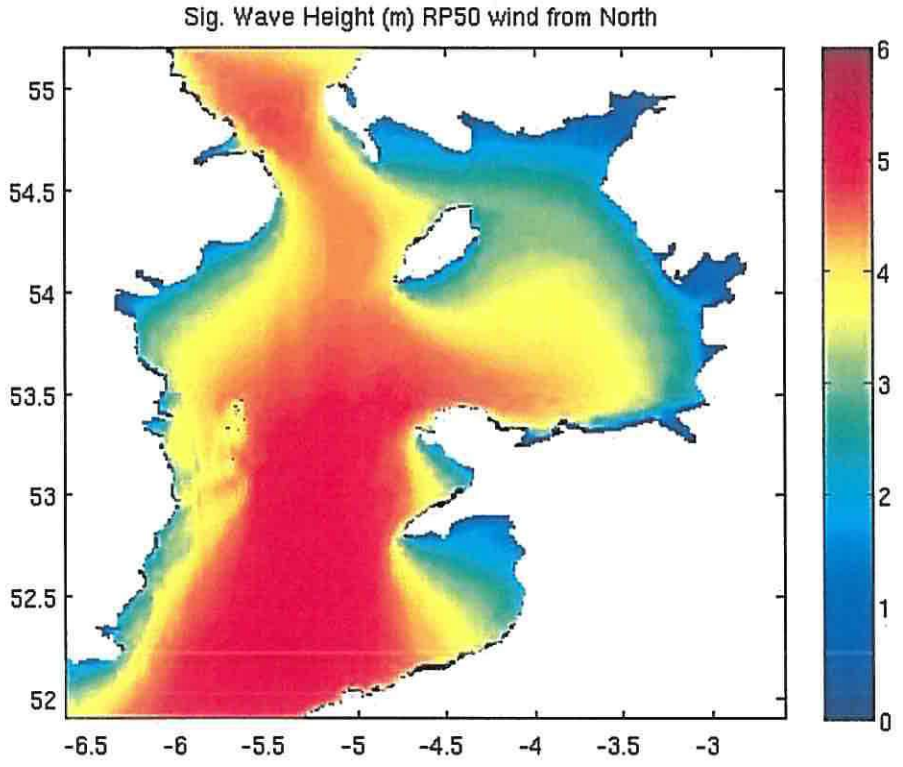
Sig. Wave Height (m) RP50 wind from North
55
54.5
54
53.5
53
52.5
52
-6.5
-6
-5.5
-5
-4.5
-4
-3.5
-3
6
5
4
3
2
1
0

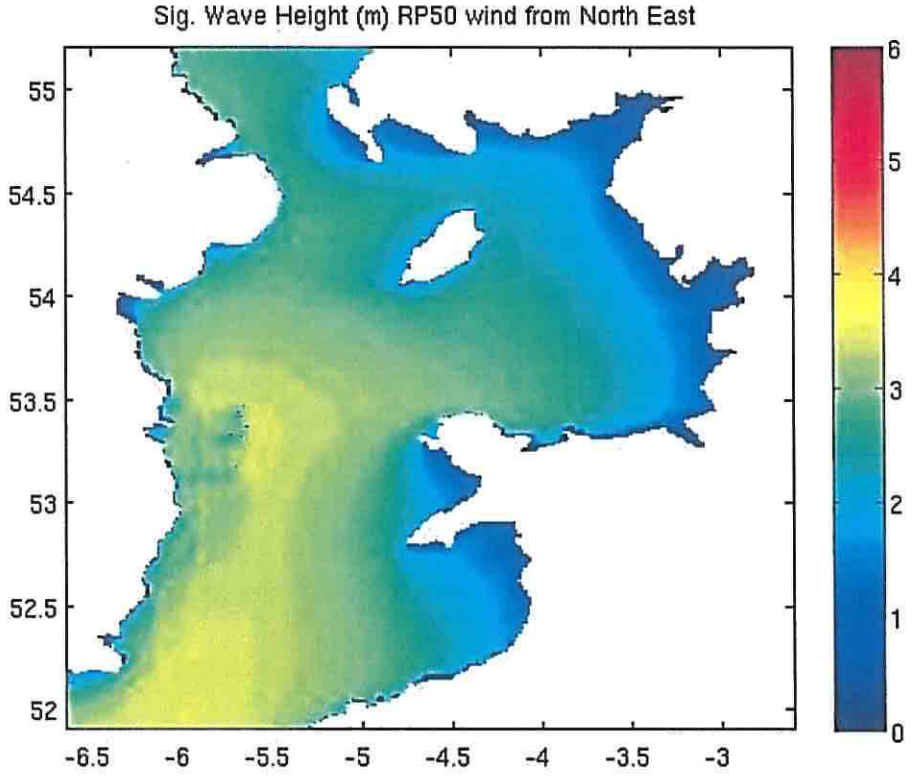
Sig. Wave Height (m) RP50 wind from North East
55
54.5
54
53.5
53
52.5
52
-6.5
-6
-5.5
-5
-4.5
-4
-3.5
-3
6
5
4
3
2
1
0

Sig. Wave Height (m) RP50 wind from East

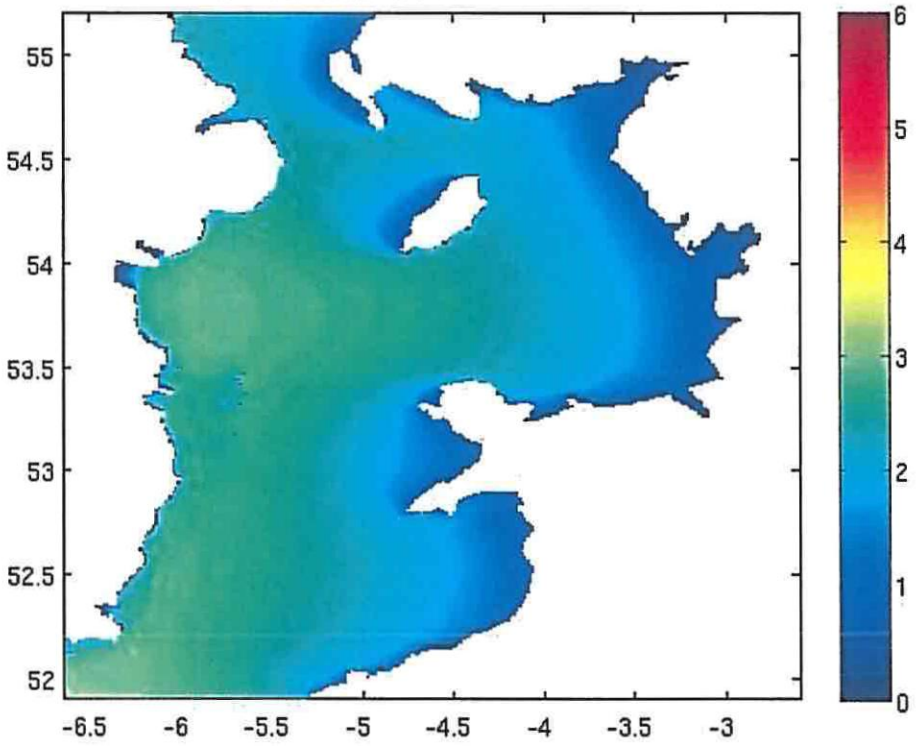

Sig. Wave Height (m) RP50 wind from South East

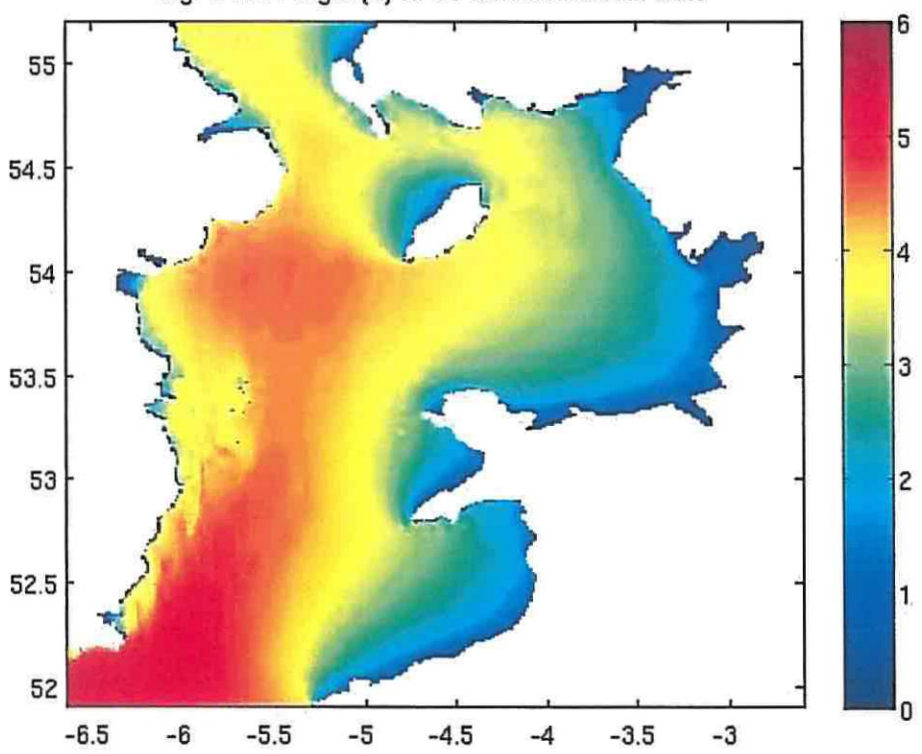

Sig. Wave Height (m) RP50 wind from South

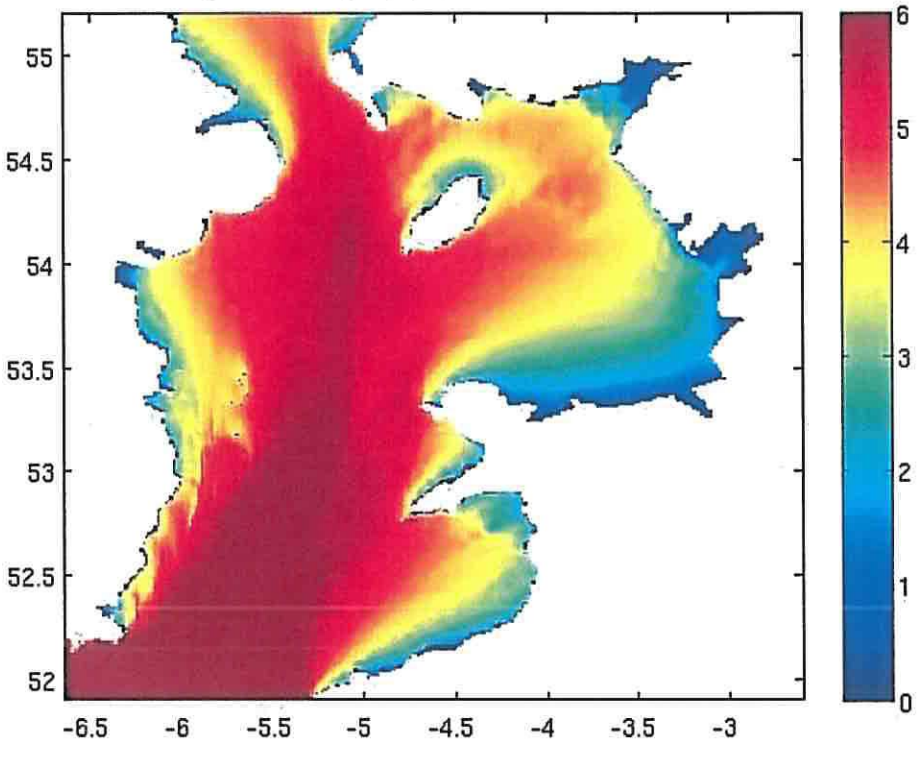

Sig. Wave Height (m) RP50 wind from South West

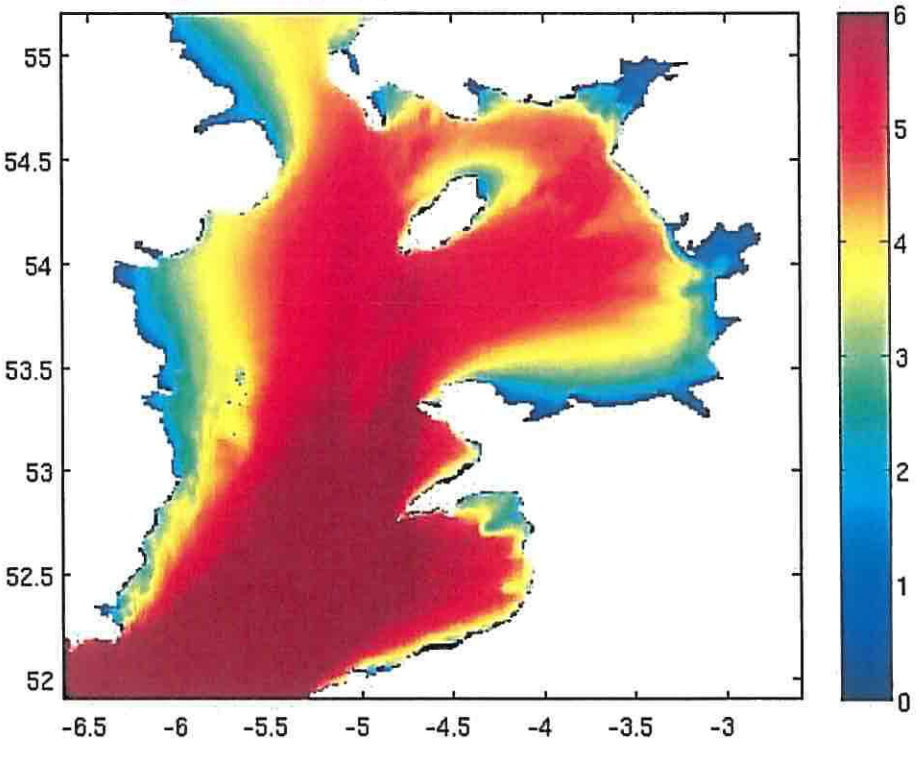

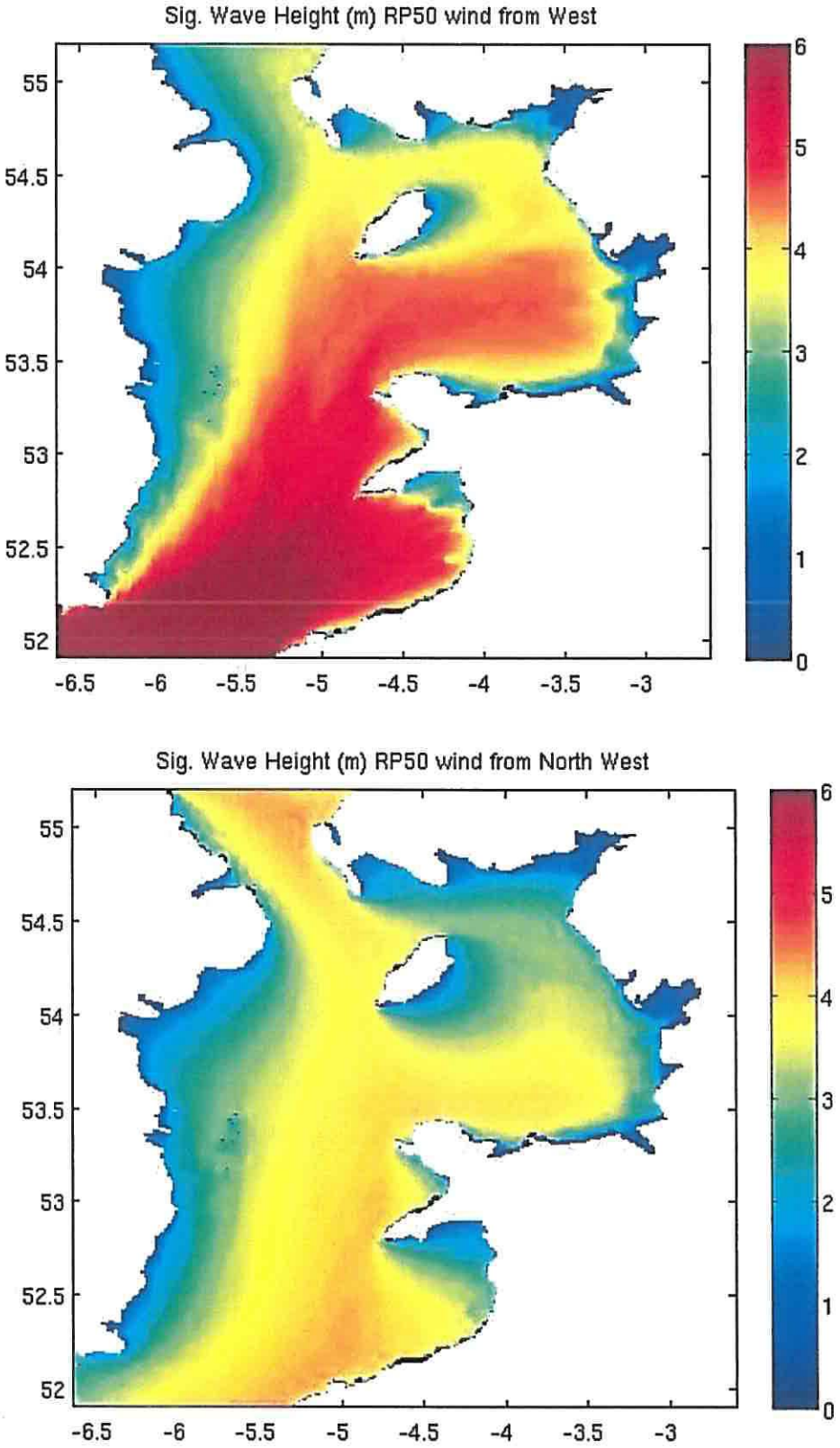

Figure 10. Significant Wave Height after steady 50 year Return Period winds from 8 sectors.

7.0 Net Forces

It was decided to model the net forces resulting from the RP50 north wind and then to compare the solutions with the RP50 south east wind. It was not clear at the outset which wind direction would result in the highest net forces, since the north wind solution for forces would be enhanced by the spring tide.

The approach to calculating the net forces was to assume that the highest wave arriving at the site would have twice the significant wave height. Such a wave would be expected to arrive approximately every 1000 wave periods, if the wave heights are fitted to a Rayleigh spectrum (e.g. the JONSWAP spectrum). This measure is commonly referred to as hmax and is often used when considering the maximum wave height and forces for engineering purposes (see for instance Holthuijsen 2007 eq. 4.2.51)

The instantaneous velocity is the sum of the tidal current and the horizontal component of the wave orbital velocity. For the purposes of the calculations here, the wave orbital velocity was calculated using linear surface wave theory and fully accounting for the water depth. The orbital velocity was calculated at a mid net depth of 2.5 m below the water surface. This was calculated at every grid point in the model domain.

We have used the method developed by Løland 1991 to calculate the response of the net as a weighted hanging screen to the instantaneous current. He postulated 2 formulae for the viscous drag and lift coefficients on flat panels:-

$$C_D(Sn,\theta)=0.04+\cos(\theta)(-0.04+0.33\,Sn+6.54\,Sn^2-4.88\,Sn^3)$$

and

$$C_L(Sn,\theta)=\sin 2\theta(-0.05\,Sn+2.3\,Sn^2-1.76\,Sn^3)$$

where θ is the angle of the flow with respect to the normal vector and Sn is called the solidity ratio and is defined as the area covered by the twines of a net and the actual area of the net:-

$$S_n=2\frac{d_w}{l_w}-\left(\frac{d_w}{l_w}\right)^2$$

where d_w is the net twine diameter and l_w is the net size. In the calculations here, we define the 'twine diameter' to include the mussels attached to the twine, so that the net solidity ratios become quite large.

These equations were determined by considering tank model test results and are therefore somewhat empirical, however they have gained widespread usage and will be used here too. Løland also put forward an equation to simulate the reduction in flow behind a net, which can be used if nets are closely spaced to give the velocity of second and subsequent nets as a geometric progression :-

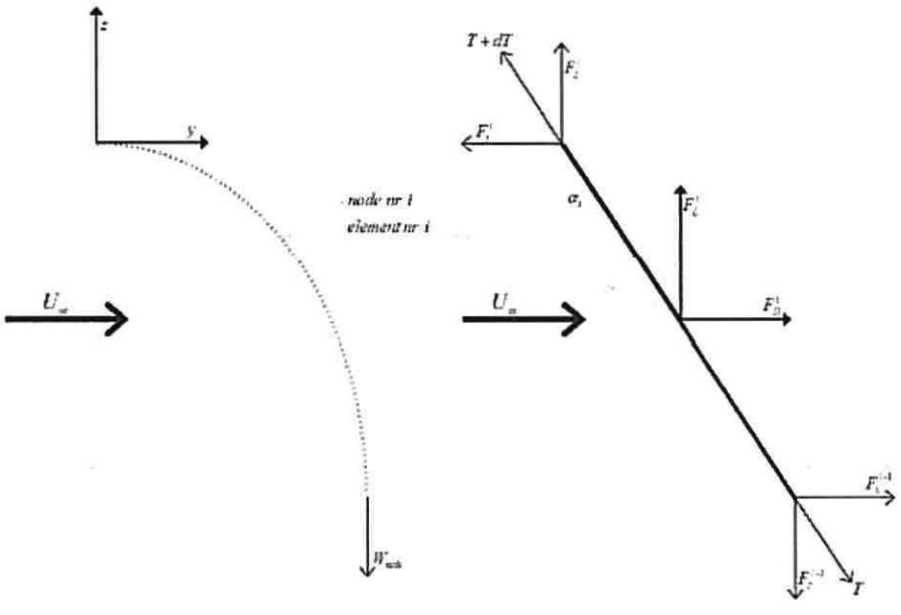

Figure 11. Diagrams showing, on the left, a vertical section through the net and on the right, the resulting drag and lift forces on an elemental length of net.

$$r = 1.0 - 0.46\,C_D$$

We have assumed here that nets do not shield each other, which is a conservative case. We have not used the r factor.

The formulae have been used to calculate both the net shape and the total tension along the net. The value of tension at the top of the net, acting horizontally (y direction in figure 11), is the uniform force used in the next stage of the calculation when we consider the shape and tension in the headrope.

The nets have dimensions 135 m long by 5 m depth. The net gauge is 0.2 m and the bottom of the nets are weighted with a total of 362.98 kg evenly distributed along the net base.

Two sets of conditions have been investigated :-

(a) The nets with seed or juvenile mussels, size 1mm.

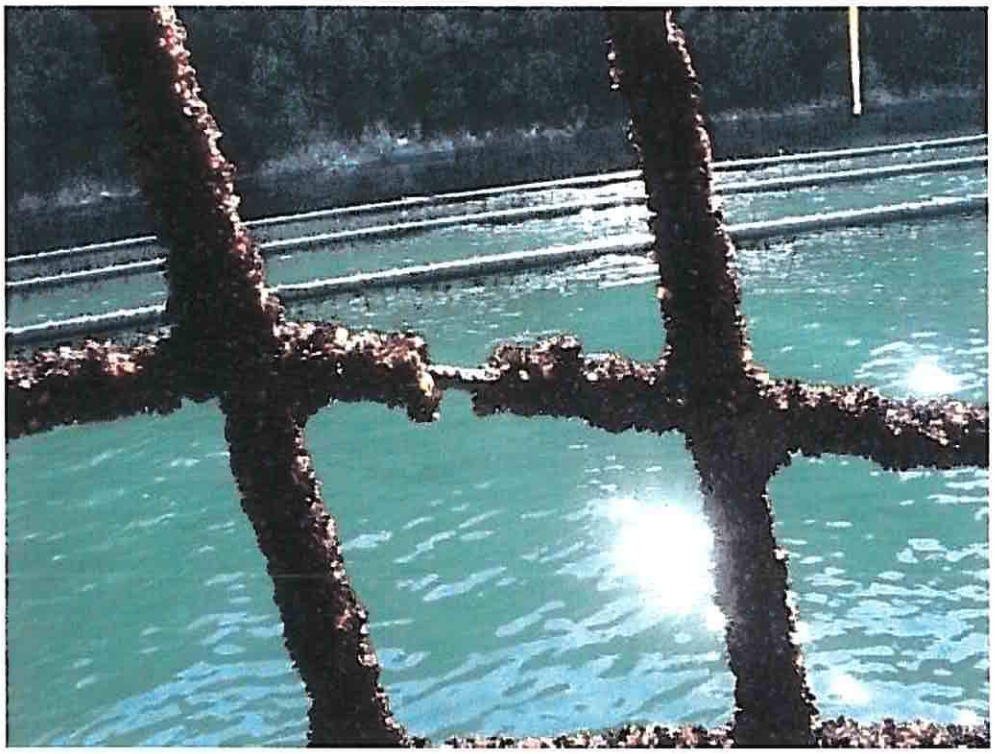

photo: SmartFarm

This corresponds to an effective 'twine diameter' = 0.018 m and a dry weight of 0.5 kg/m of net rope corresponding to 2,564 kg per net. This was adjusted to be 20% of the weight to account for their buoyancy.

(b) Pre-harvest mussels of size 80-90 mm.

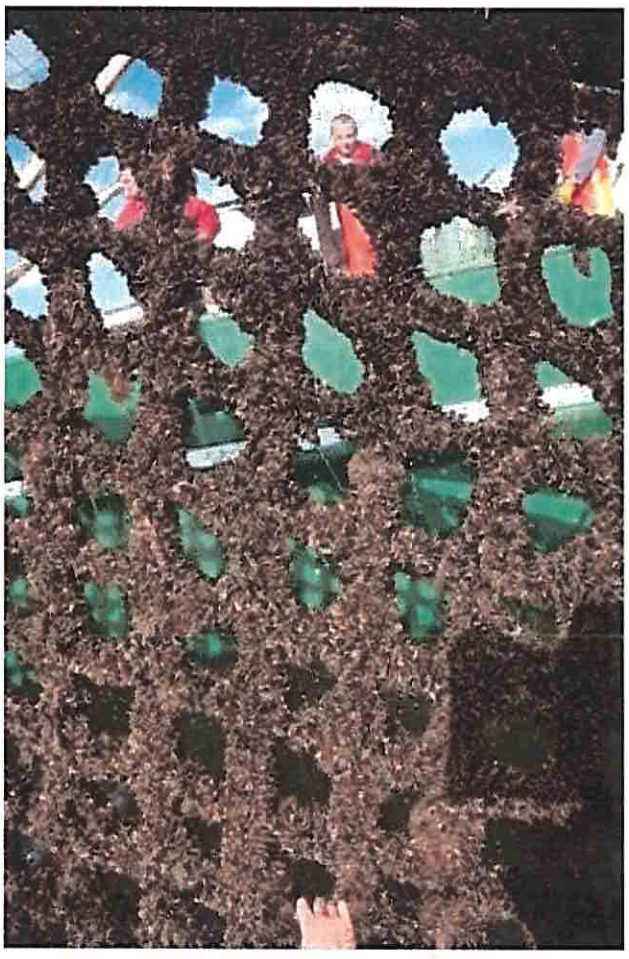

photo: SmartFarm

This corresponds to an effective 'twine diameter' = 0.08 m and a dry weight of 4.5 kg/m of net rope corresponding to 20,073 kg per net. Again, this was adjusted to be 20% of the weight to account for their buoyancy.

The nets are arranged with a separation of 10m. There are 55 net units in the roughly east-west direction (the exact angle is used in the calculation) and 4 in the roughly north-south direction.

The net unit configuration fits well into the prospective license area with a border of 30 m to the east and west of the outermost nets. Screw anchors are positioned 60 m from the buoys marking the ends of the headropes. There is a margin of 10 m between roughly east-west rows of anchors. As part of this study, the exact positions of each anchor are delivered as an electronic spreadsheet. We have used the 60 m anchor scope here, since the screw anchors can sustain a considerable vertical pullout force as well as a horizontal force. The anchor positions are shown in figure 12.

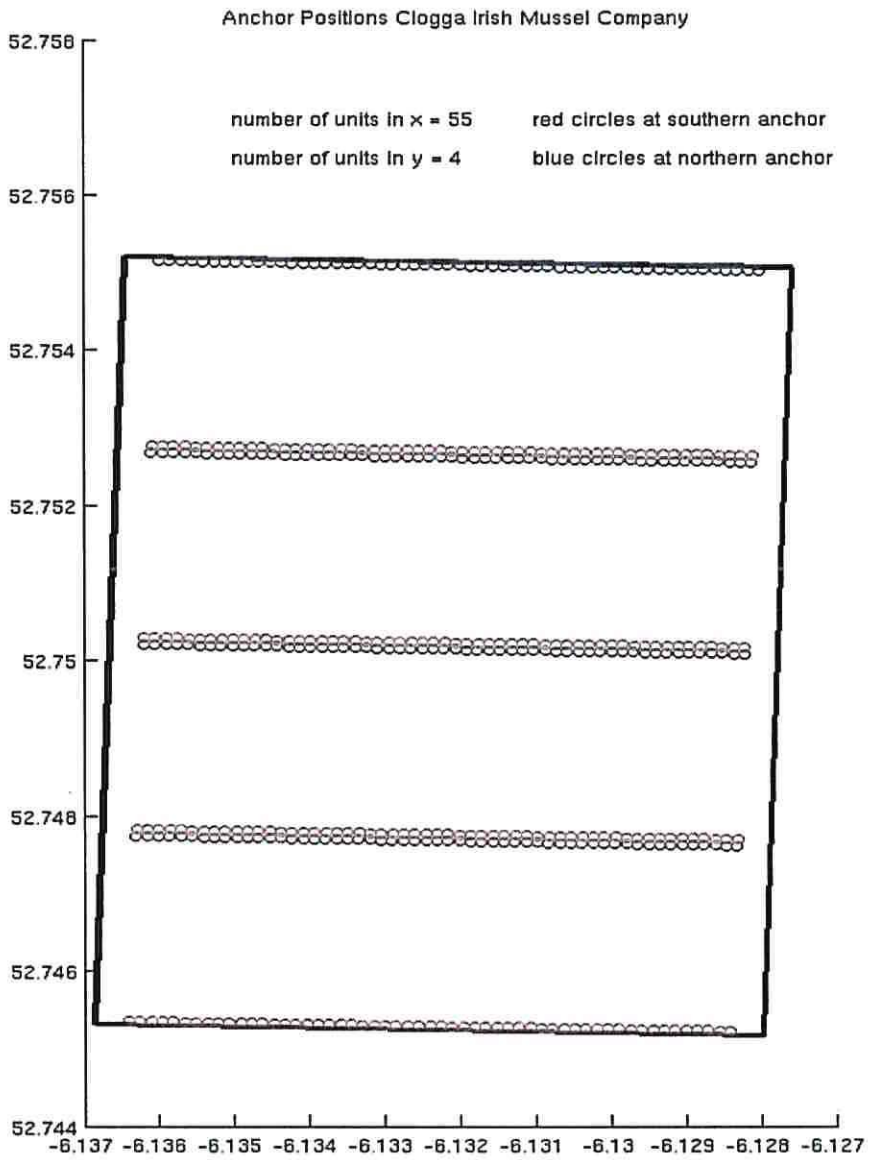

Figure 12. Anchor positions for the Clogga site. The black outline shows the proposed license area.

The central position of each net was used to interpolate the steady current vector and the instantaneous horizontal wave orbital velocity vector from the model grid output at the maximum southerly spring tide flow (in the case of the RP50 north wind experiment), or the maximum northerly spring tide flow in the case of the RP50 south easterly wind simulation.

For the RP50 wind simulations for each wind direction, the model data is interpolated onto the 55x4 net layout. The comparison for the north wind and the south east wind simulations are shown in figures 12-17. These figures show how the total velocity is calculated at the mid-depth position of each net. It can be seen that the wave velocity component is much larger than the steady tidal current. The total velocity is the sum of the horizontal component of the instantaneous wave orbital velocity and the hydrodynamic current (principally the tide). The peak value of this velocity is similar for both the north wind and the south east wind cases, but the location is very different. For the north wind case, the net units at the southern end all experience the high velocity of 3.1 ms^{-1}, but for the south east wind case, only the net units in the extreme north west, located in a very shallow corner experience the 3.2 ms^{-1} velocity.

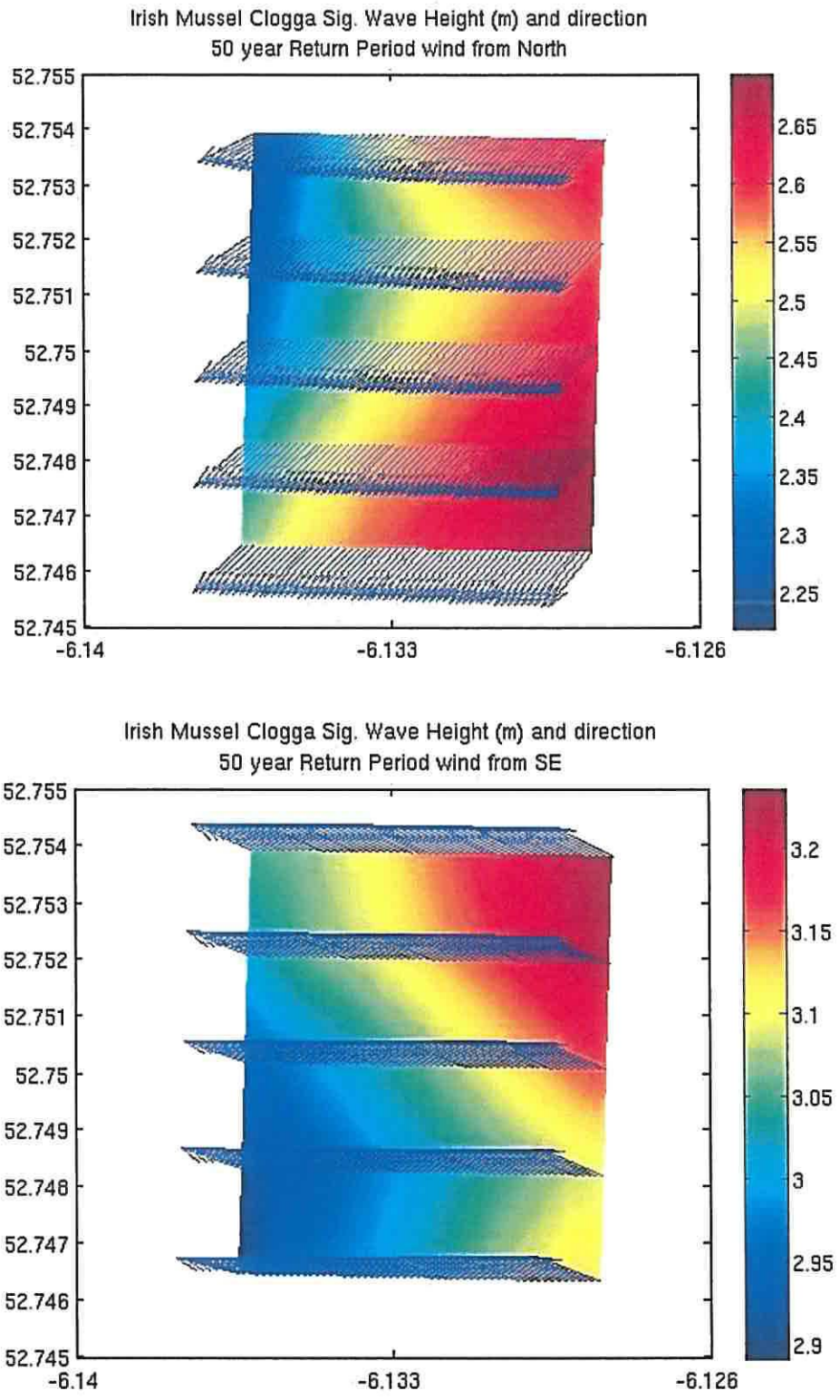

Figure 12. Significant wave height and wave direction at each net unit for the RP50 north wind and south east wind simulations.

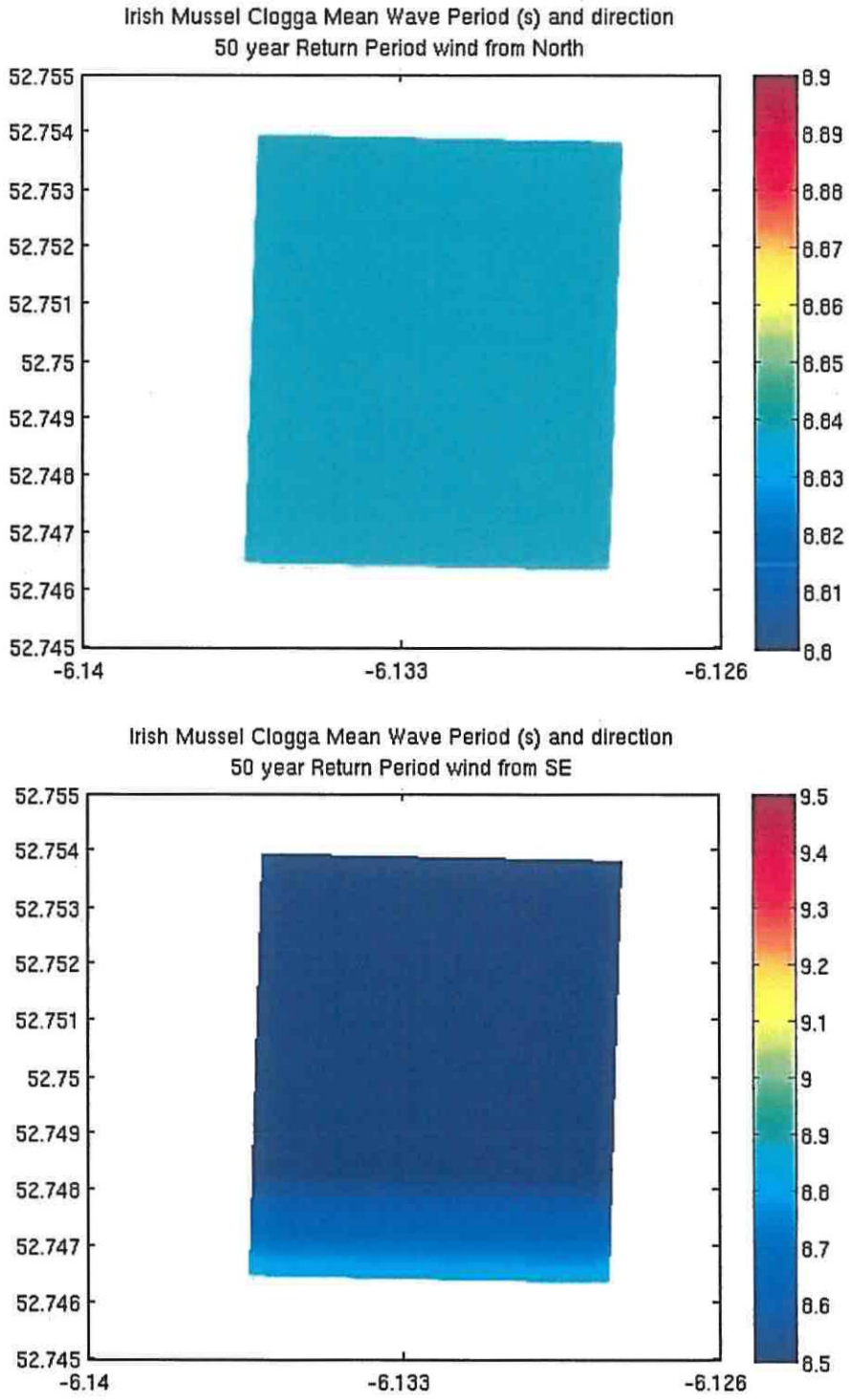

Figure 13. Mean Wave Period at each net unit for the RP50 north wind and south east wind simulations.

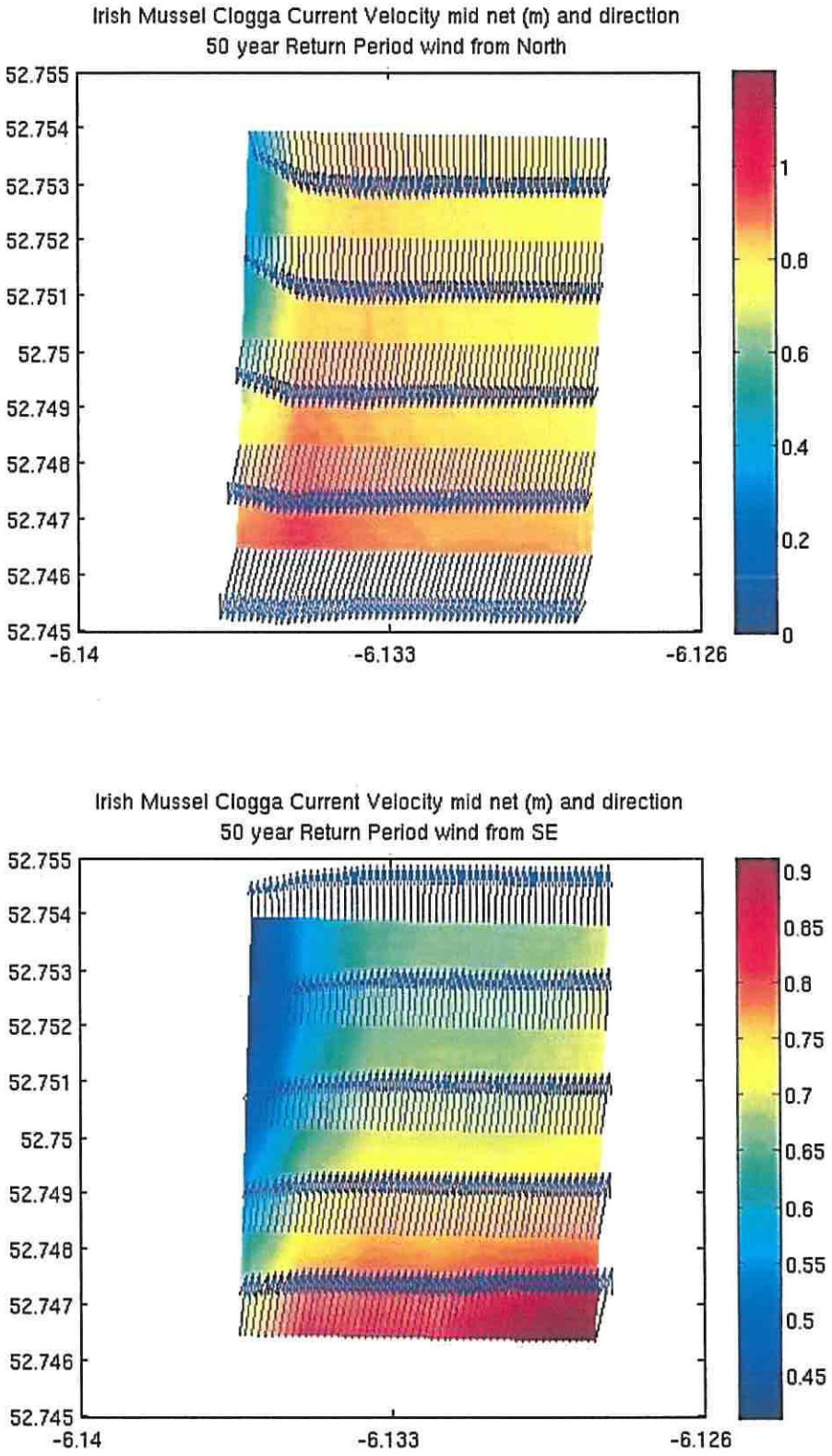

Figure 14. Tidal current interpolated to a depth of 2.5 m corresponding to the mid-depth net level for the peak spring tide and the RP50 north and south east wind simulations.

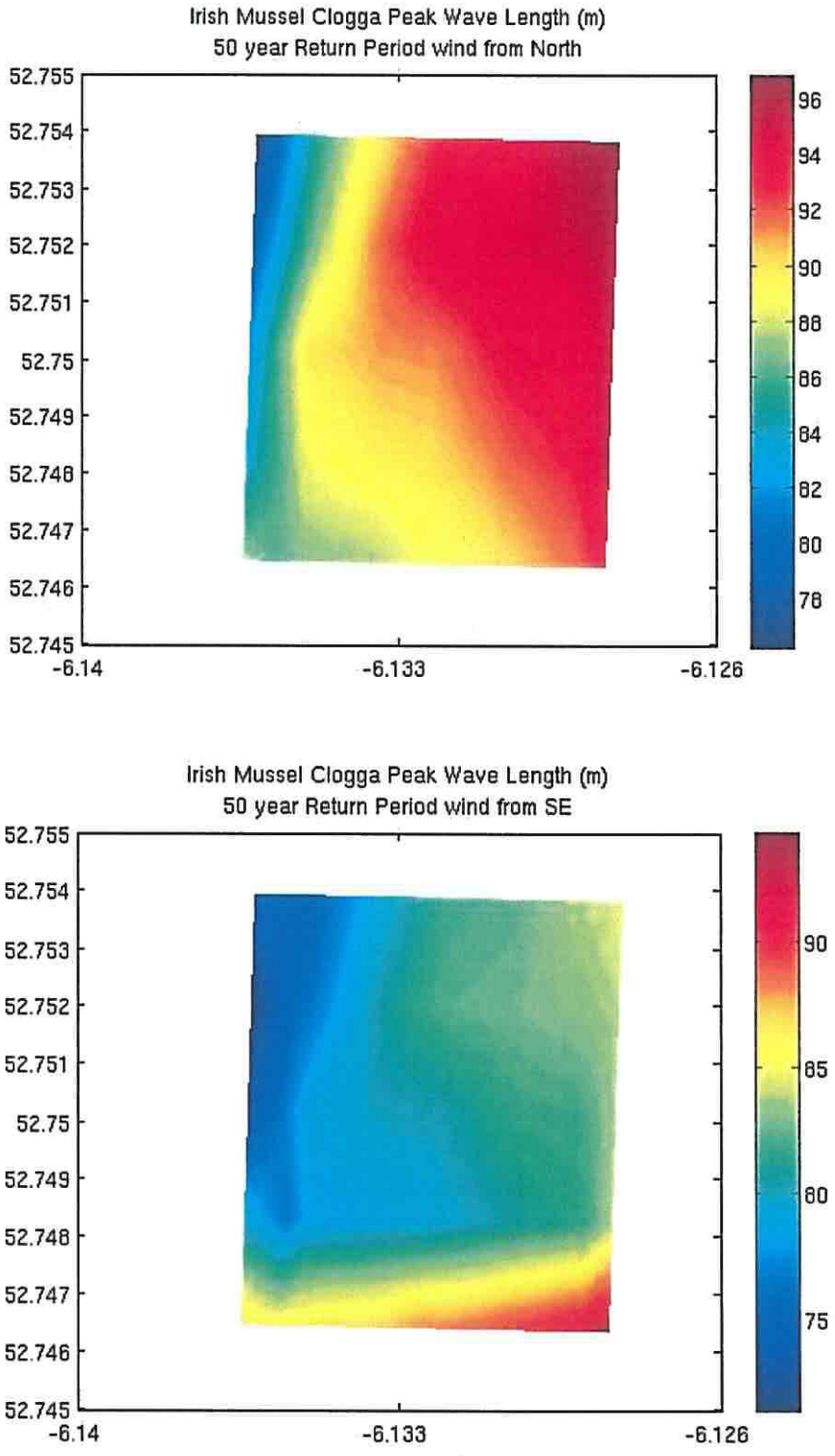

Figure 15. Peak wave length of the surface waves for the RP50 north wind and south east wind simulations.

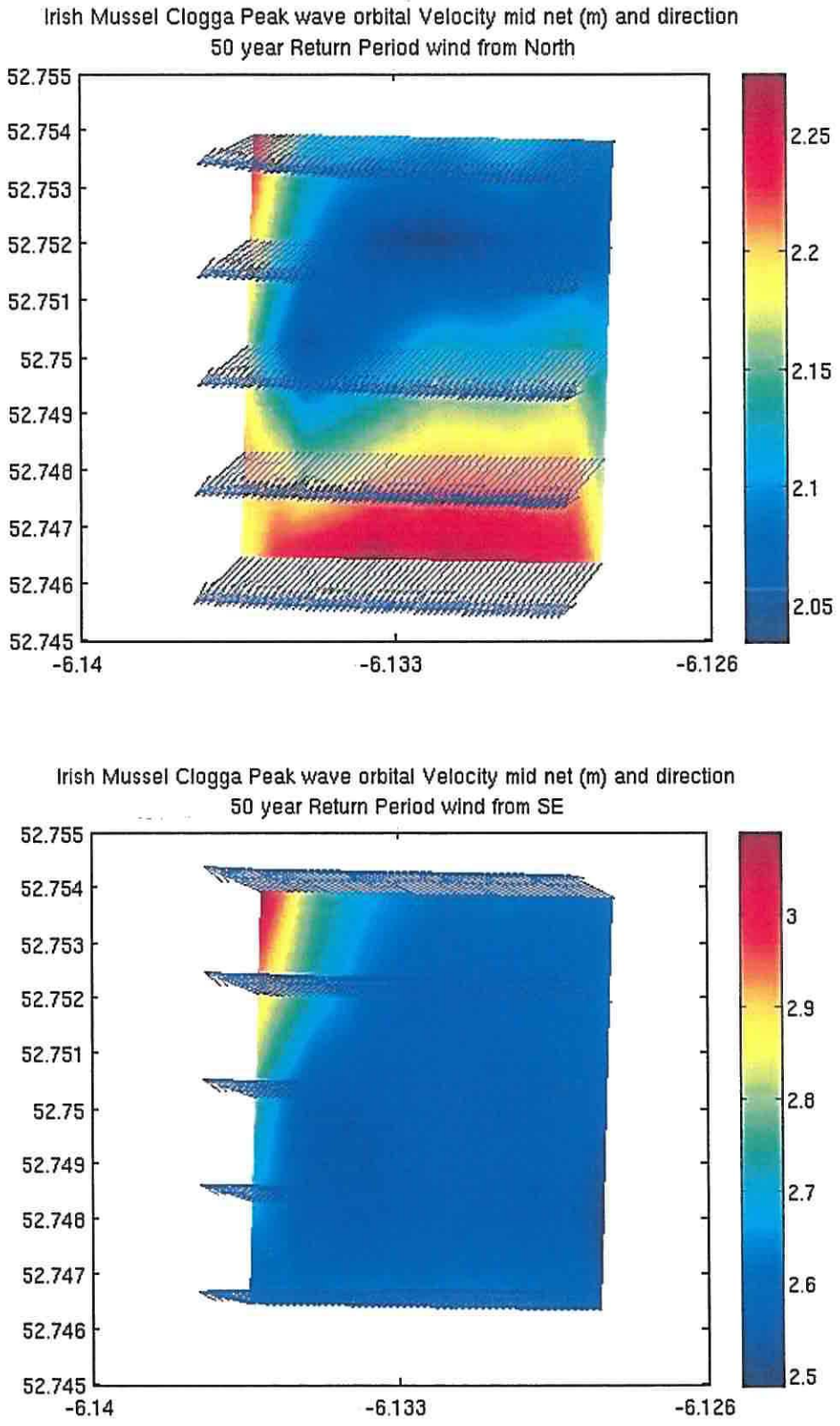

Figure 16. Maximum horizontal wave orbital velocity calculated at 2.5 m depth coresponding to the mid-depth of the nets for the north wind and south east wind simulations.

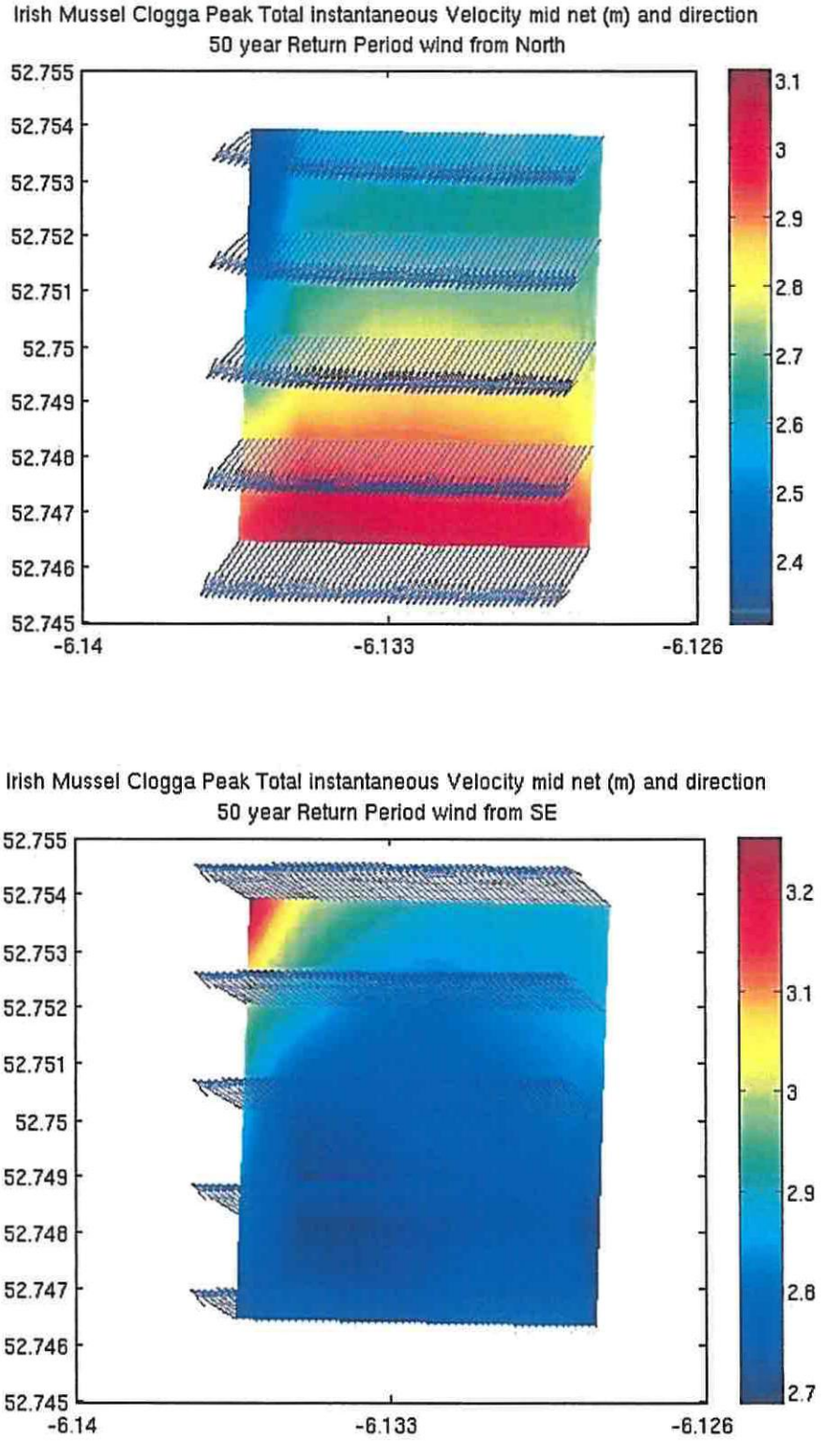

Figure 17. The total velocity as the sum of the wave orbital and the tidal current at the mid -depth of the nets for the north wind and the south east wind simulations.

Using the total velocity, we calculate the vector component perpendicular to the net and then use Løland's formulae to calculate the net shape and tension distribution over the depth of the net. The net shapes are shown in figures 18 and 19 for both the juvenile and mussel laden nets and the pre-harvest laden nets. We show the situation for that net group subject to the maximum current for both the north wind and the south east wind cases.

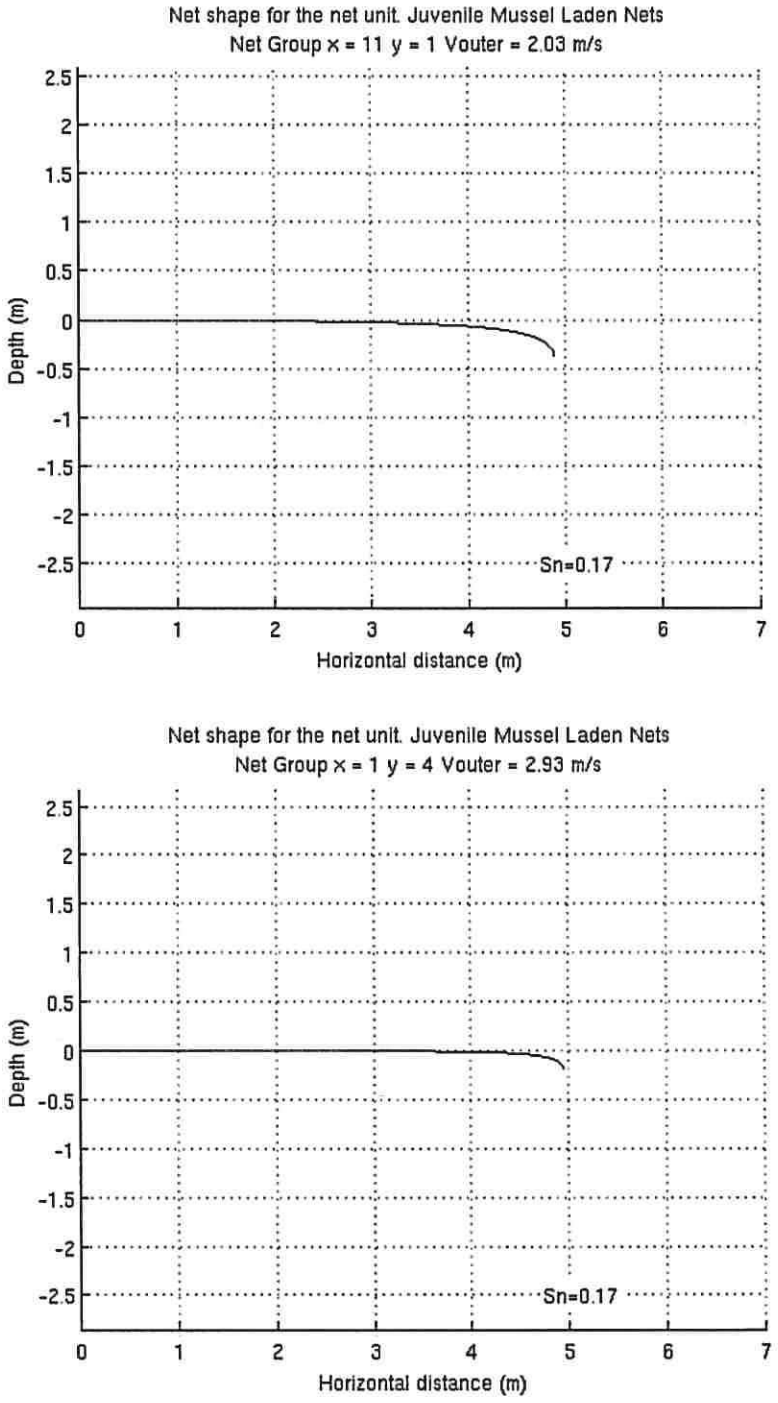

Figure 18. The shape of the net units subject to the maximum combined wave and tidal currents. For the RP50 north wind, the net group position is x=11, y=1 (upper) corresponding to the net group along the southern edge of the site. For the RP50 south east wind, x=1, y=4 (lower) corresponds to the NW corner.

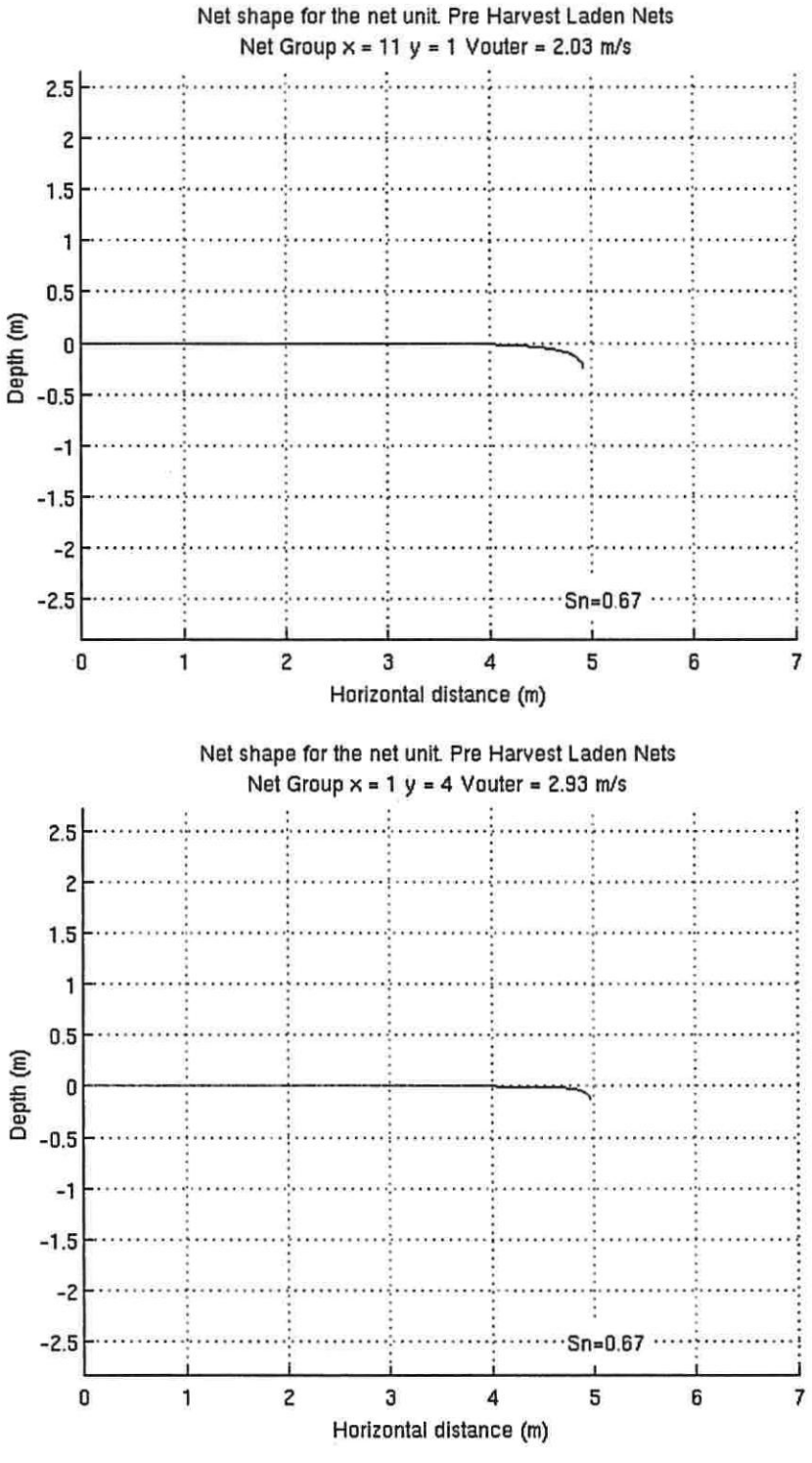

Figure 19. Same as figure 18, but laden with pre-harvest mussels.

It is clear that the nets are adversely affected by the instantaneous current to the extent that they are almost horizontal in the peak currents. The reason that the pre-harvest nets are worse, even though they have a higher mass of mussels, is because the net solidity factor is much higher and the mussels have considerable buoyancy.

In order to show the full range of solutions, we also show the net shapes for the net units subjected to the lowest curents for both the north wind and the south east wind cases. These are shown in figures 20 and 21. We see that the nets are behaving better at this location, but are still fairly horizontal. In figures 22-25 we show the net tension distribution.

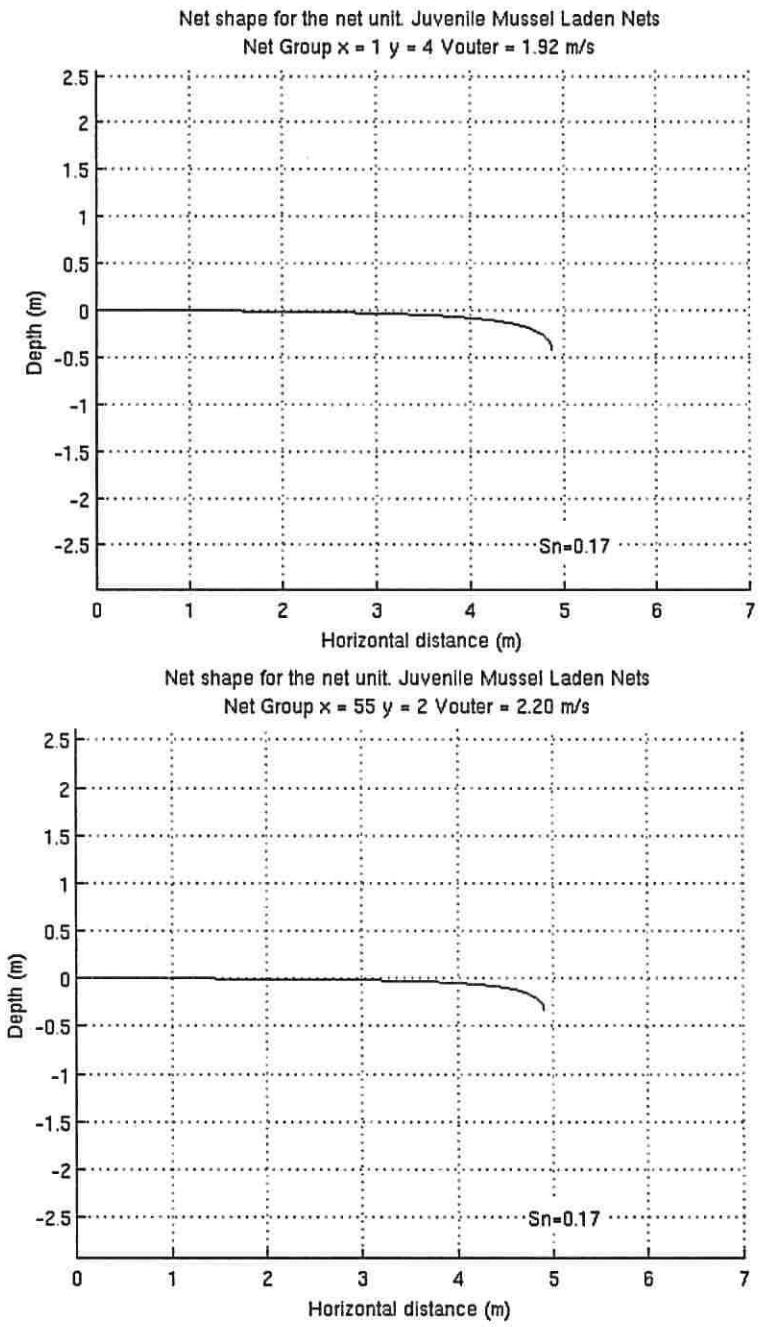

Figure 20. Net shapes for the juvenile laden net group subject to the lowest instantaneous current for the north wind and the south east wind cases.

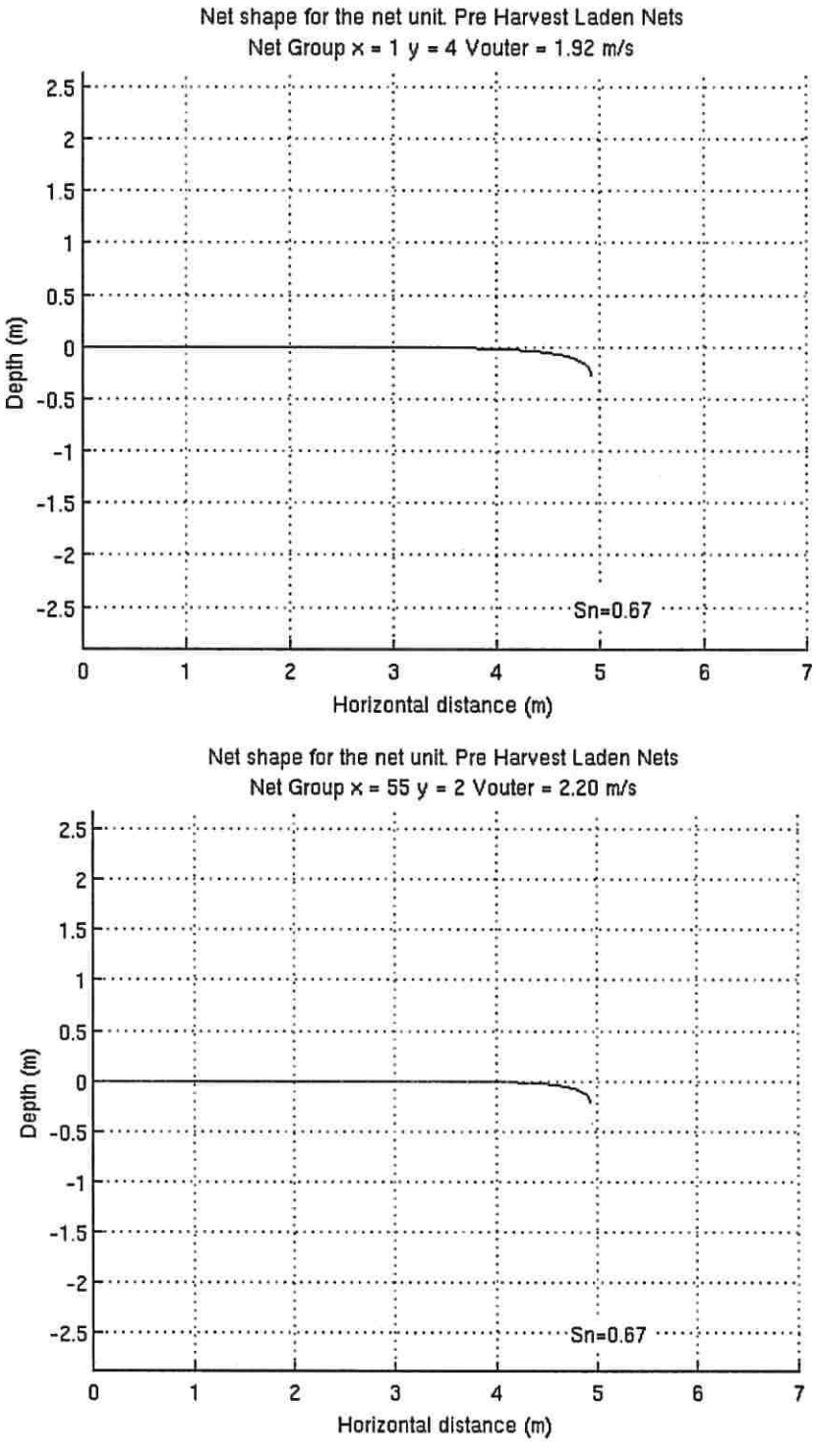

Figure 21. Same as figure 20, but for the pre-harvest laden nets.

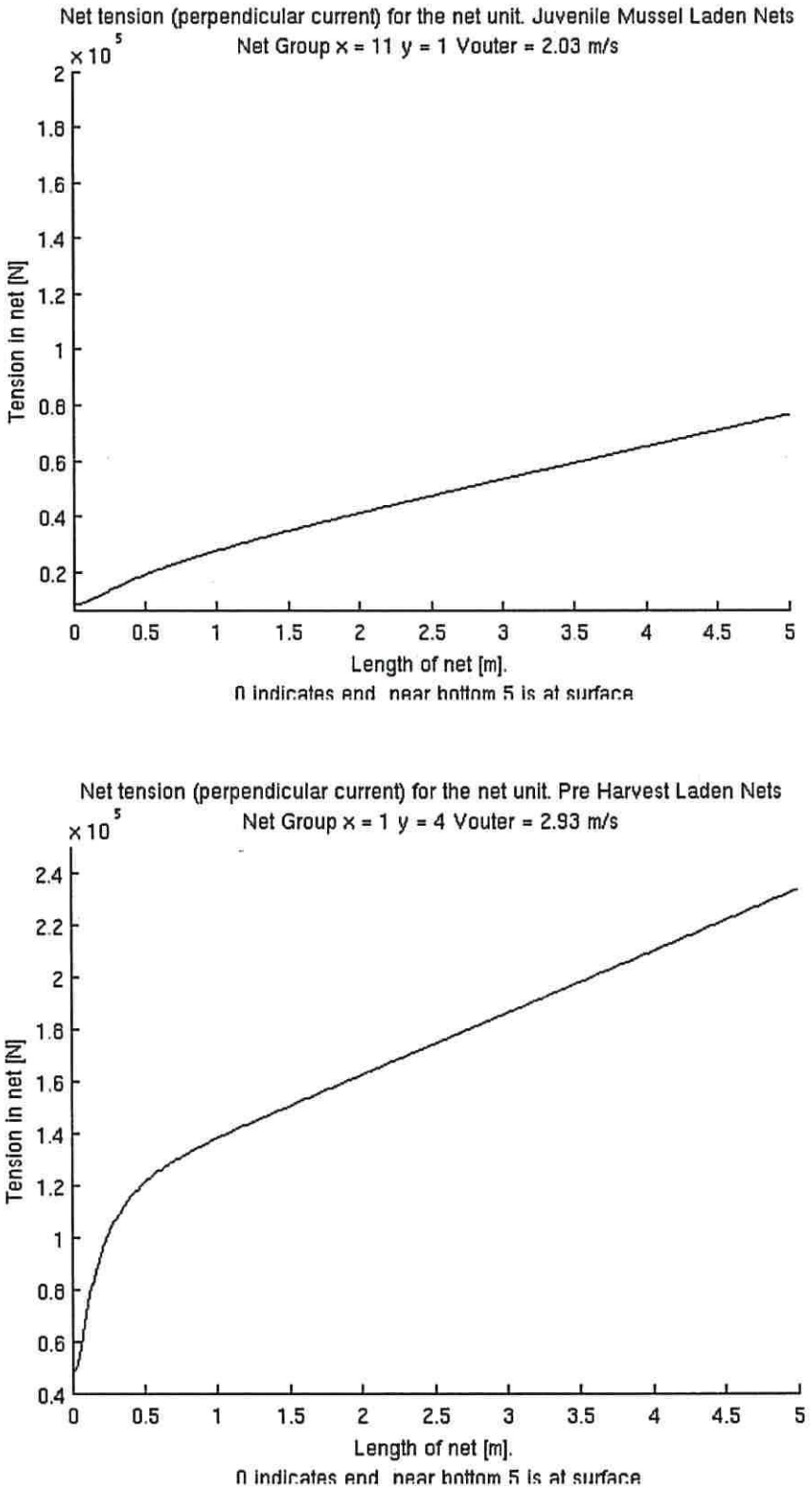

Figure 22. Tension in the net for the juvenile laden case and the high current position in the site. Both the north wind (upper) and the south east wind simulation cases are shown.

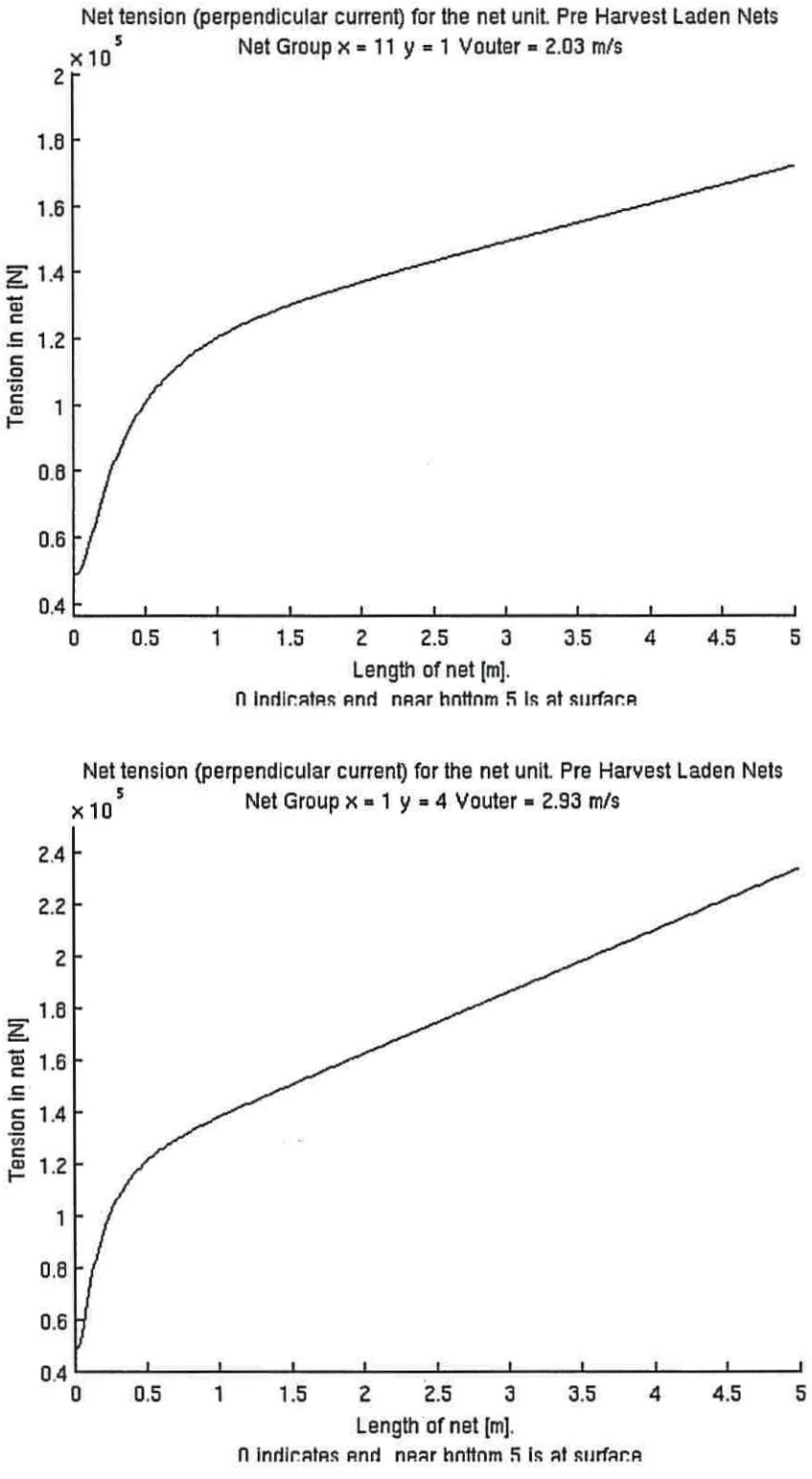

Figure 23. Same as 22 but for the pre-harvest situation.

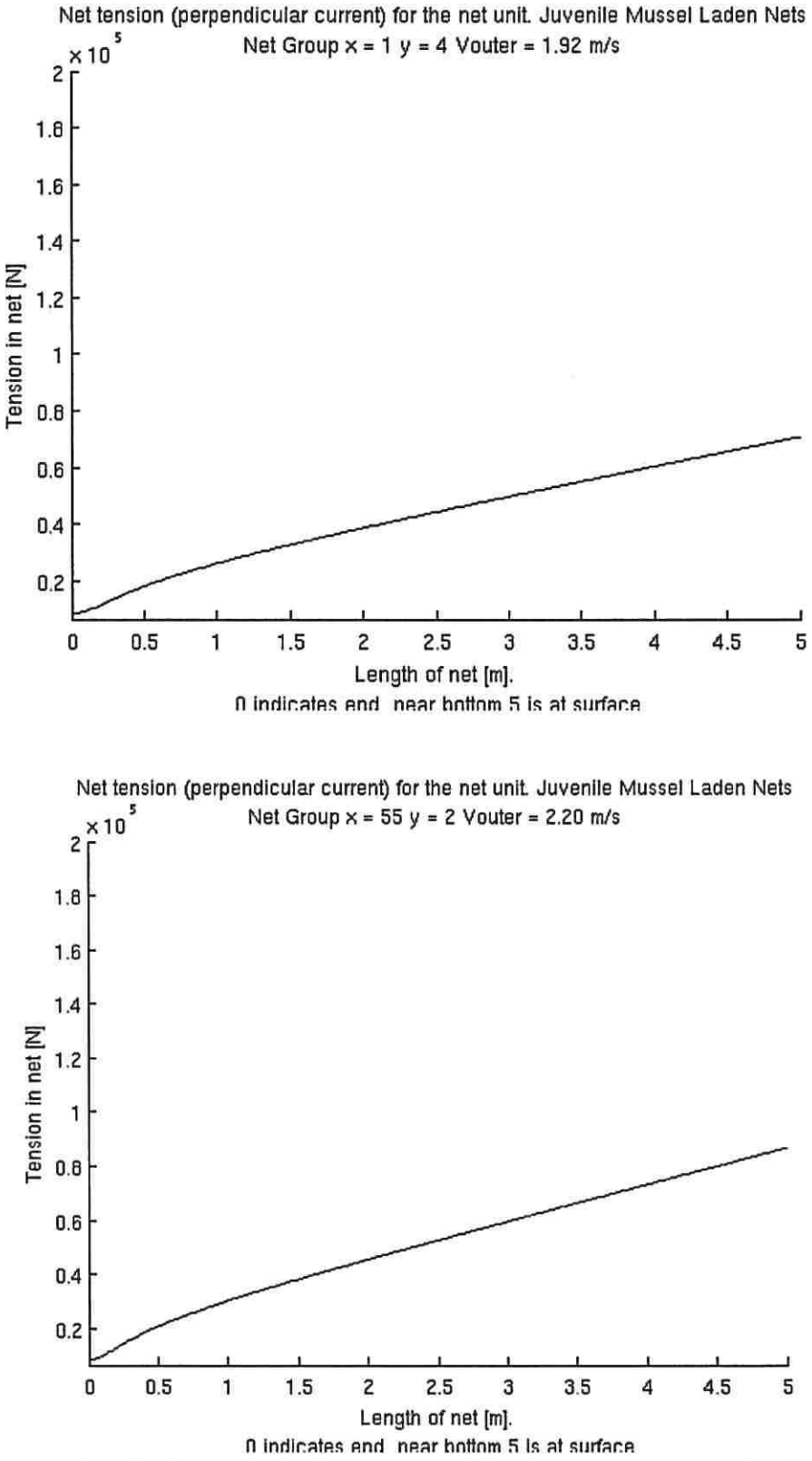

Figure 24. Net tension for juvenile laden nets and for the net group at the lowest current position in the site. RP50 north wind (upper) and south east wind simulations are shown.

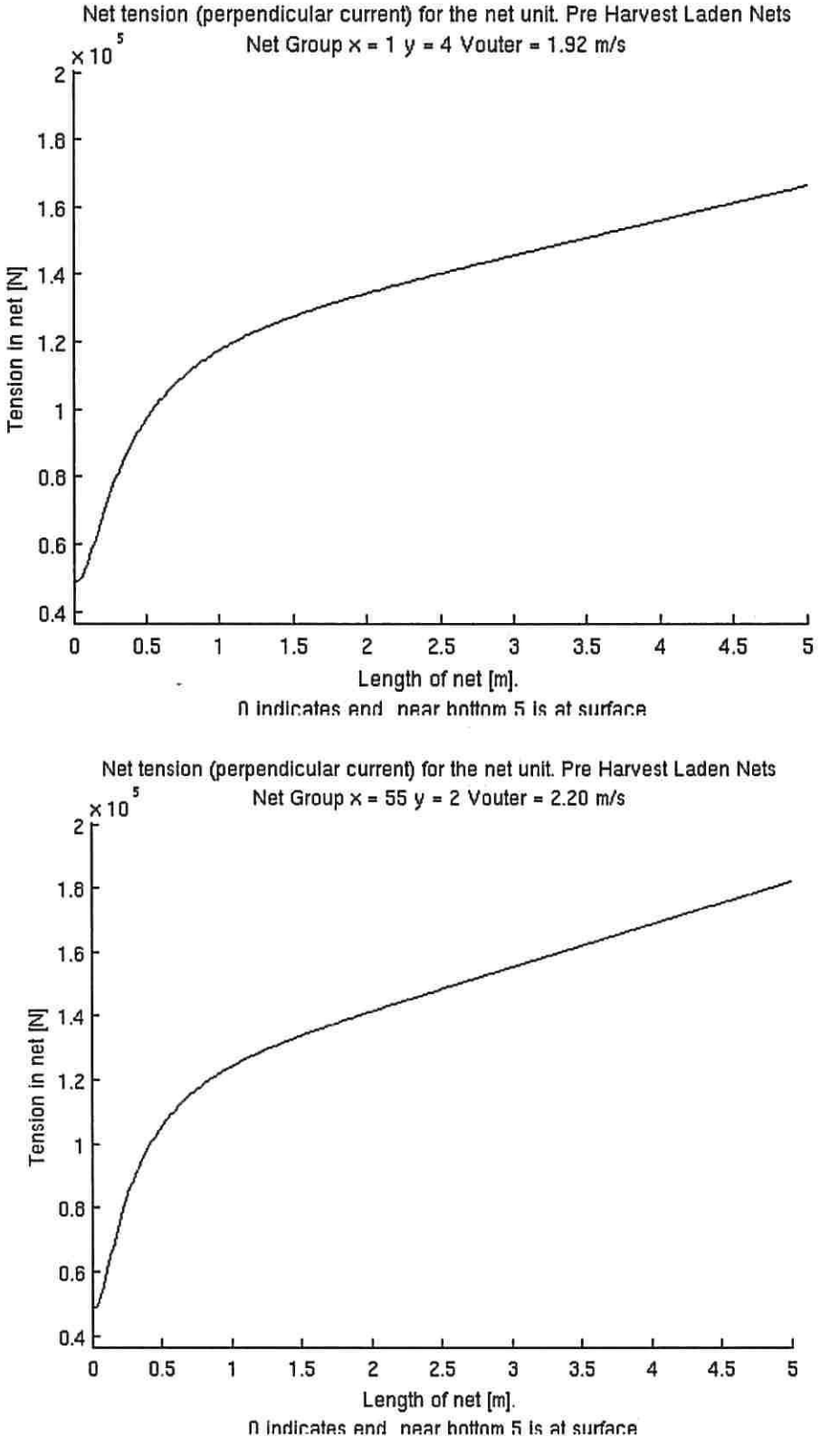

Figure 25. Same as fig. 24, but for the pre-harvest situation.

We can calculate the tension due to the net deformation using Løland's formulae for each net unit. This force acting perpendicular to the net, is transmitted to the headrope at the sea surface. This will act to deform the headrope and to stretch it. One of the concerns is that this outermost net will then touch the adjacent net. We wish to calculate this headrope deformation and in particular what mooring force will be required to prevent it touching the adjacent nets.

The following headrope parameters are used :- rope material polypropylene, with diameter 0.09 m and Young's modulus of elasticity = 7.0×10^9 Nm-2. This last figure came from a study of rope properties by Weller et. al. 2013.

The design criterion was that the net should not deform by more than 15 m at its mid point. The total net length is 135 m and there is an additional 5 m of headrope on either end, so that the total headrope length is 145 m. Each net will have a different extension to preserve the prescribed mid point deformation.

Figure 26 shows the headrope shape for the highest current position on the site and for the pre-harvest case.

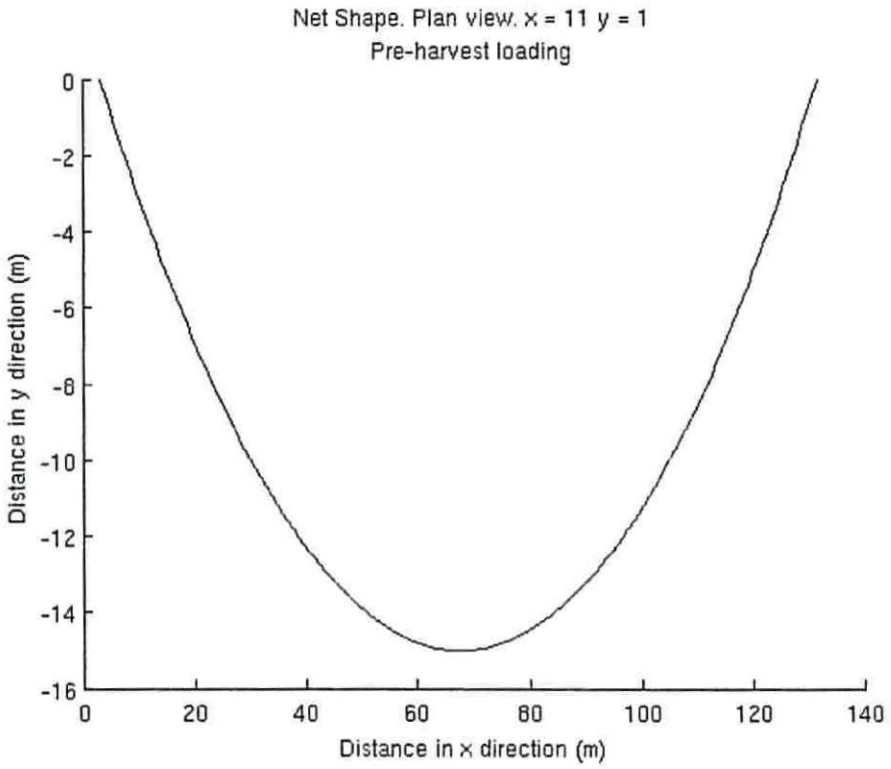

Figure 26. Plan view of the headrope shape for the high current preharvest case and the north wind simulation.

So far we have only considered the lateral force on the nets. For the force along the undeformed net axis, we simply treat the net as a series of vertical pipes and use a simple drag force calculation :-

$$F_X = 1/2 \rho U^2 C_D A$$

where A is the cross sectional area in the plane of the flow, ρ is the water density taken as 1026 kgm^{-3} and C_D is a drag coefficient set to 0.17 (information supplied by SmartFarm AS).

We have not included any reduction in drag due to shielding of net twines, since the net is assumed to take a three dimensional shape and therefore this force will be a conservative estimate. As will be see, this force contributes much less than the lateral force to the mooring tension.

If we calculate the forces for each net unit and then add this to the tension caused by the waves and currents acting laterally to the nets, we arrive at the total mooring line tension

for each net unit. We show the contribution of the waves and the steady tidal currents to the mooring tension and then the total mooring tension.

These are plotted as grids for the juvenile and the pre-harvest cases in figures 27-32.

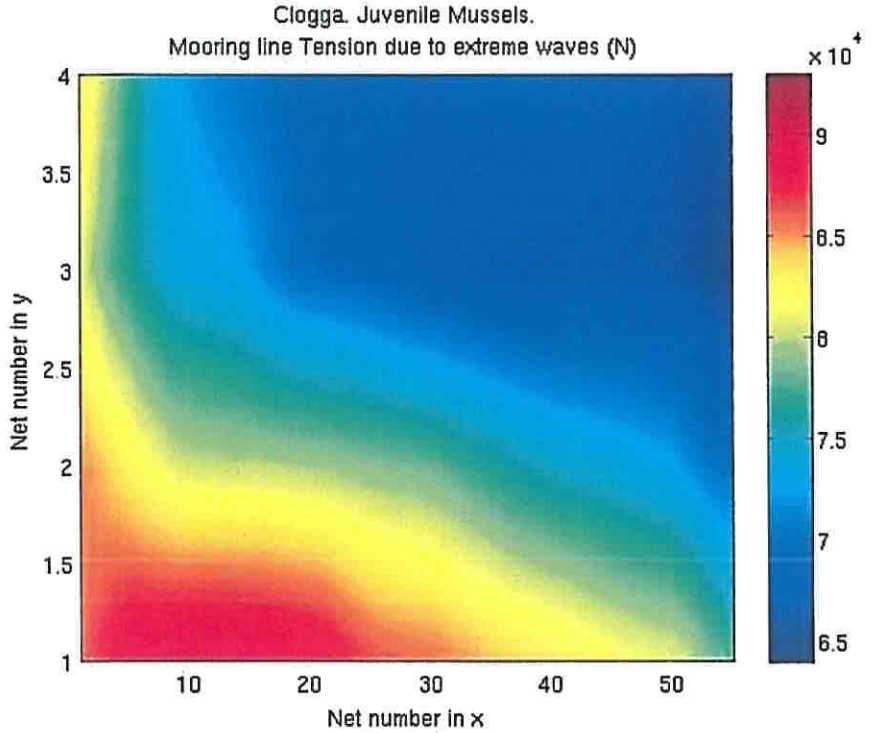

Figure 27. Mooring line tension due to extreme waves for the juvenile case. RP50 north wind simulation.

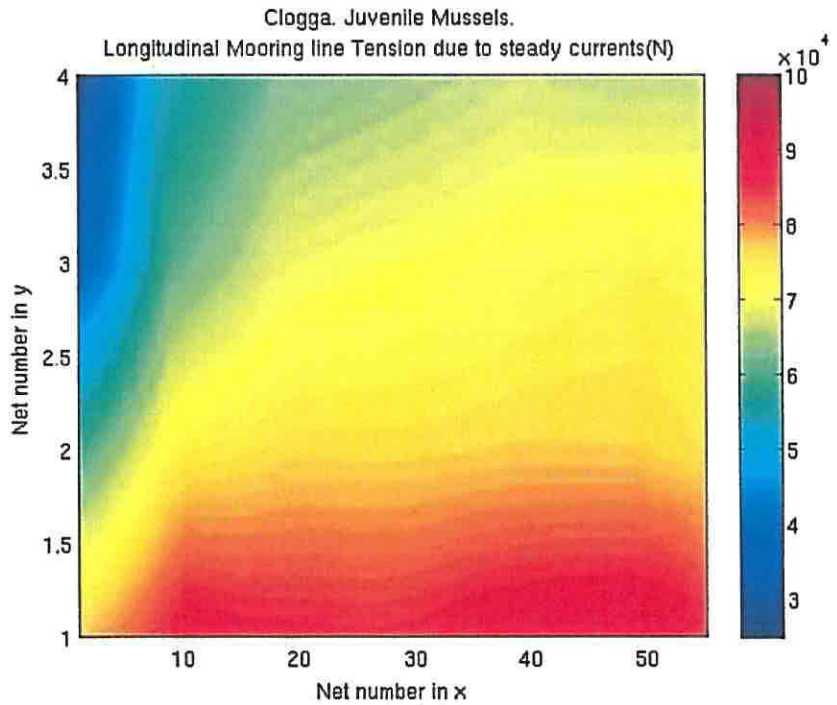

Figure 28. Mooring line tension due to currents for the juvenile case. RP50 north wind

simulation.

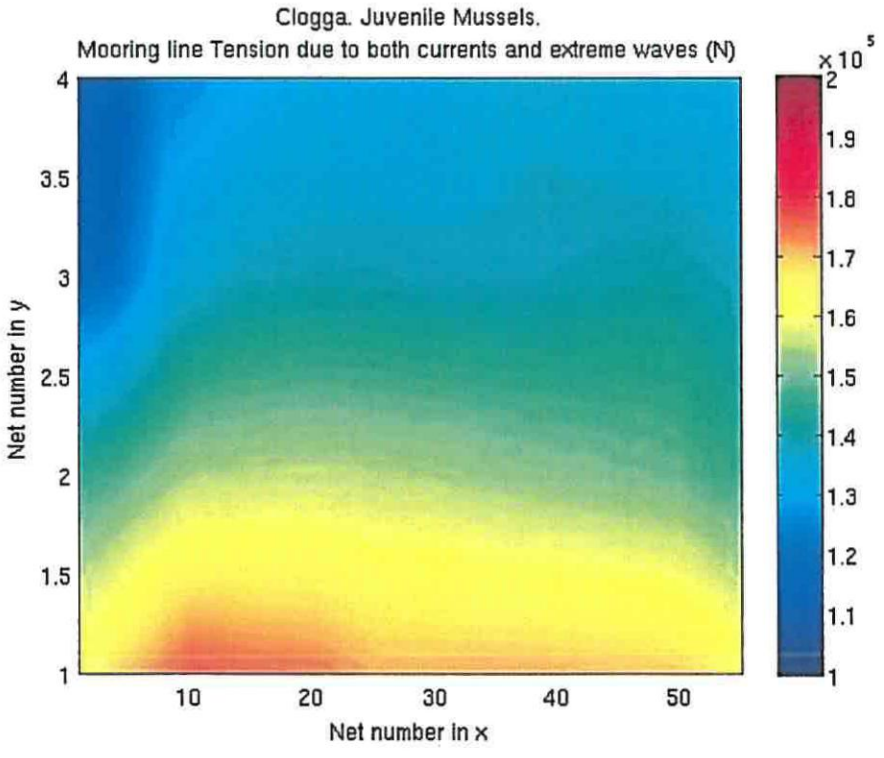

Figure 29. Total mooring line tension due to extreme waves and currents for the juvenile case. RP50 north wind simulation.

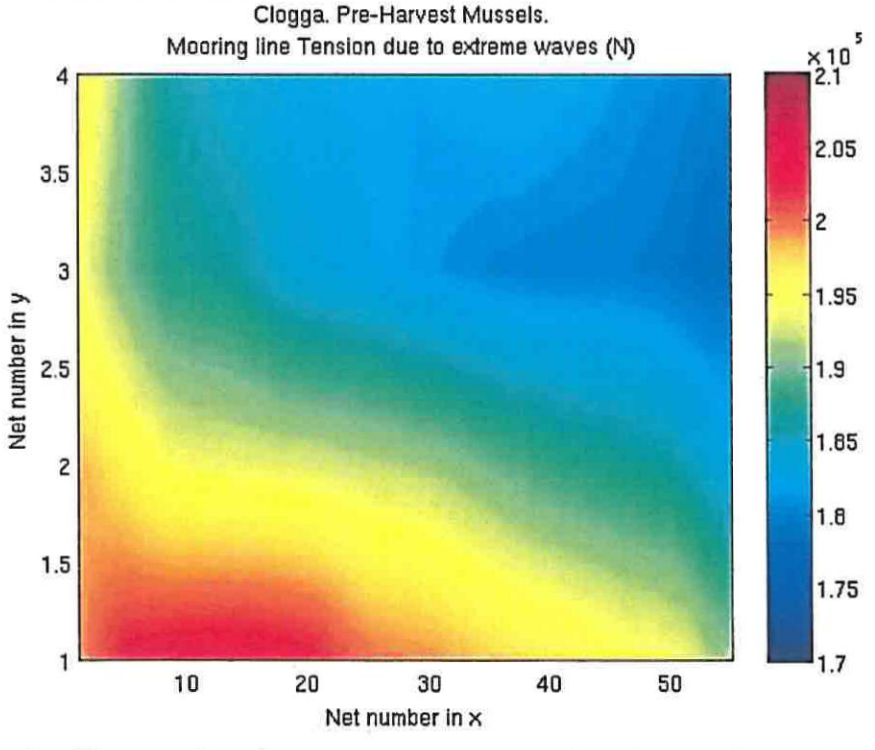

Figure 30. Mooring line tension due to extreme waves for the pre-harvest case. RP50 north wind simulation.

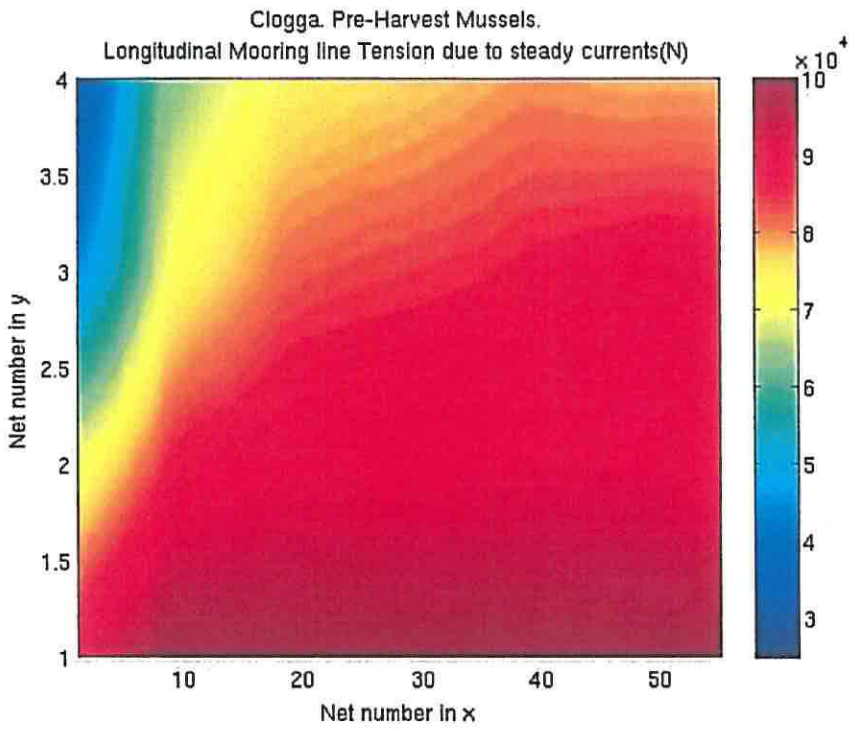

Figure 31. Mooring line tension due to currents for the pre-harvest case. RP50 north wind simulation.

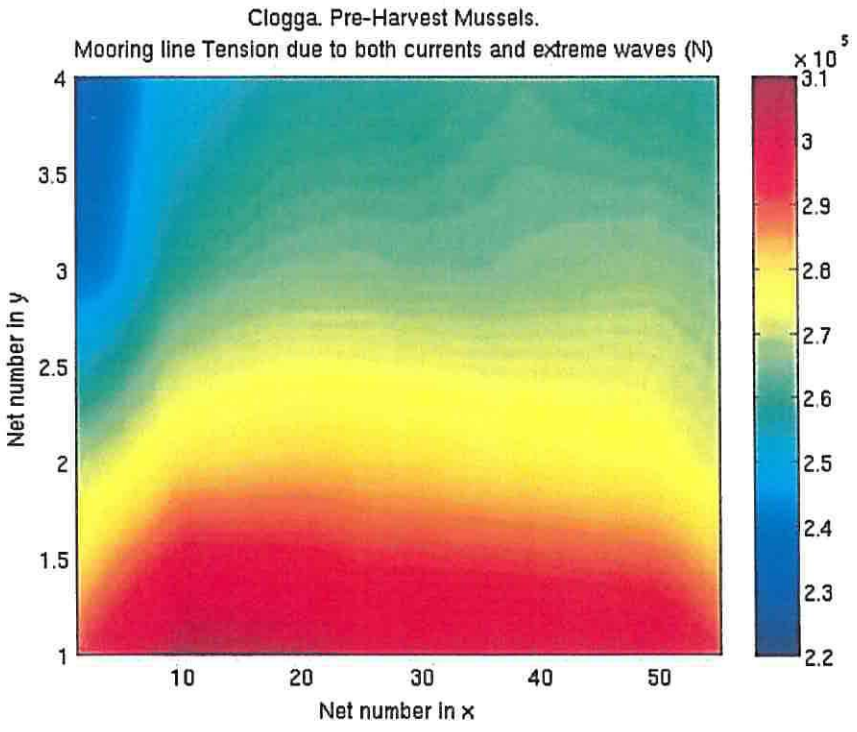

Figure 32. Total mooring line tension due to extreme waves and currents for the pre-harvest case. RP50 north wind simulation.

It can be seen that the mooring line tension for the pre-harvest situation varies between 229 kN and 310 kN. This compares with the figure of 2948 kN derived by Arup in their

analysis. The reason the figures are much lower is that the headropes have been allowed to deform considerably in their response to the forces.

The headrope stretch does not exceed 2.0% and so is well within the plastic limit of the polypropylene rope (about 20%). The distribution of net stretch for the pre-harvest case is shown in figure 33.

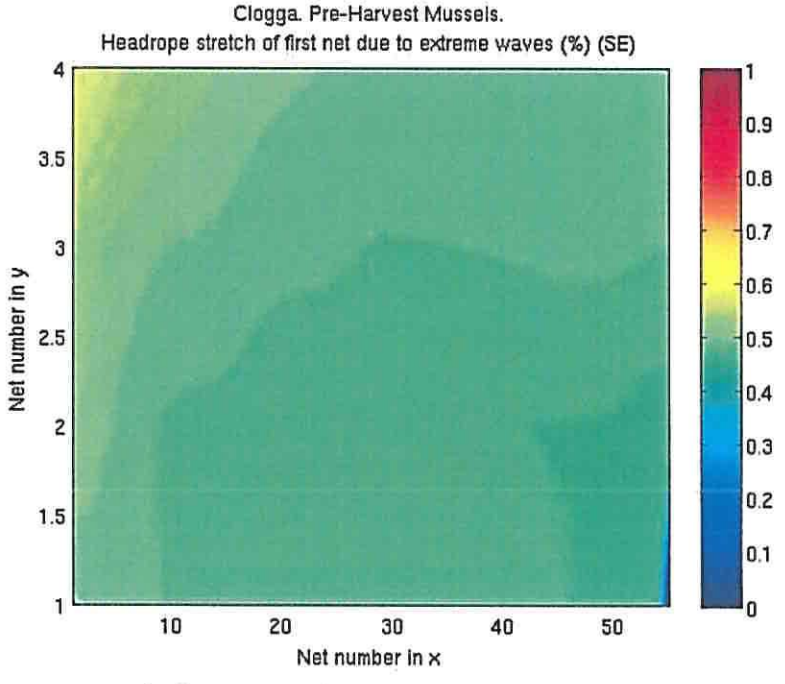

Figure 33. Headrope stretch due to total forcing of waves and currents for the RP50 SE winds.

Finally we show the total mooring tension for the case with RP50 south east wind and pre-harvest mussels in figure 34.

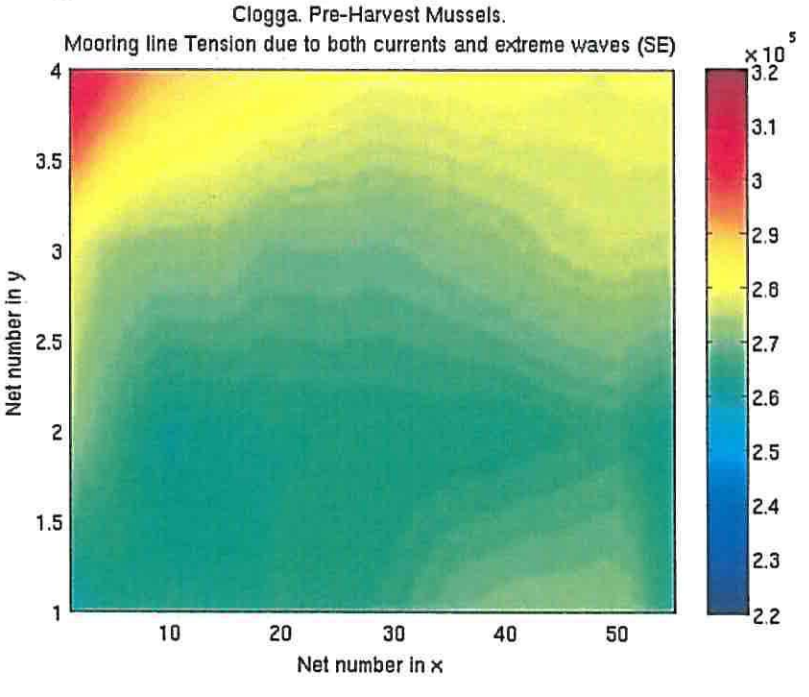

Figure 34. Total mooring line tension for the pre-harvest case and RP50 south east winds.

The mooring line tensions have a different distribution from the RP50 north wind case and the tension in the mooring line varies between 261 kN and 318 kN. The tensions and their range are very much the same as for the RP50 north wind case.

8.0 Mooring Calculations

The moorings comprise a screw anchor, a chain of length equal to the one half of the mean depth at that position plus 60.5 m and a surface buoyancy tube at the headrope. The specification of the anchor will depend on the forces calculated here. The chain used for the calculations has a diameter of 0.03 m and a weight of 18.5 kgm^{-1}. The breaking load of the chain is 115.3 tonnes. The surface buoyancy tube has a total length of 135 m and one half of this has been assumed to act as the buoyancy on each mooring. The buoyancy tube has a diameter of 0.335 m.

The method used for the mooring calculations splits the mooring into its individual components each with a drag coefficient and projected area into the fluid flow We also prescribe the Youngs modulus (or elongation under load), buoyancy and weight. The chain component is split into 1 m lengths and the drag and weight of each length are summed. If the force on the mooring is such that the surface buoyancy is overwhelmed, then it becomes a sub-surface mooring and the tube will adopt a sub-surface position. The drag on the buoyancy tube will then be included in the mooring calcualtion.

For the calculations here, we analyse each mooring individually and in the first instance we look at the mooring shape with no hydrodynamic load, but instead only a static lateral tension of 100 KgF. The reason for this static load is to maintain the headrope's linear shape when not under force from waves and currents. We then calculate the mooring shape under the extreme loads of waves and currents for each of the RP50 wind directions.

One of the aims was to have the anchors lined up neatly in order to utilise the space within the licence area efficiently. By looking at the 'no load' condition we can see that we maintain the scope of the anchors of approximately 60 m and that a portion of the chain lies along the sea bed.

Figure 35 shows the no load condition for the anchor at x=11, y=1, which is the position of maximum force under the RP50 north wind simulation. Figure 36 shows the same mooring subjected to the extreme load. Now the mooring is taut and there is a small angle between the chain and the sea bed at the anchor. The uppermost end of the mooring has now been moved in the direction of the force, so we need to make sure that it will not interfere with the adjacent net unit and mooring.

Since the anchor is a screw anchor, it can sustain a pullout force. The screw anchors will be designed for the predicted vertical and horizontal forces in the most extreme position and RP50 waves and currents.

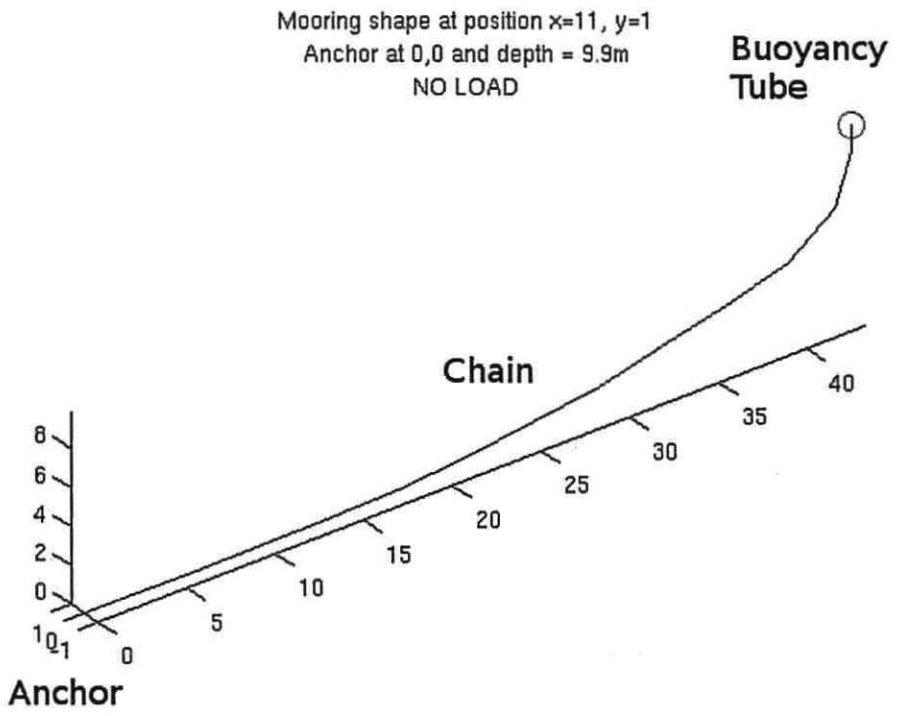

Figure 35. Mooring shape for the no load conditon at x=11, y=1 with the RP50 north wind. The buoyancy tube sits at the sea surface 10.2 m above the sea bed.

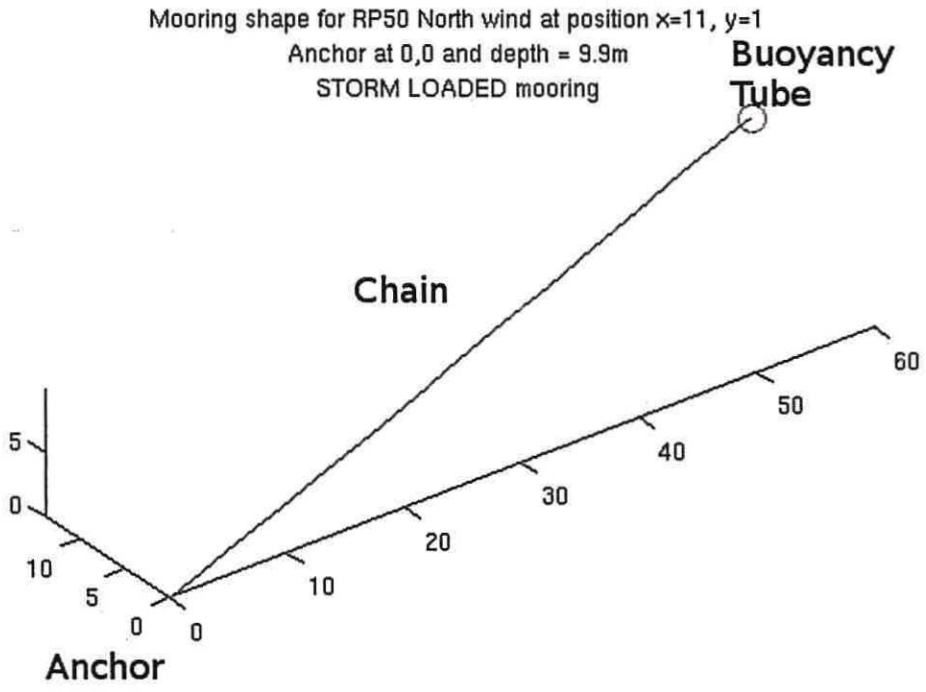

Figure 36. Mooring shape for the load conditon at x=11, y=1 with the RP50 north wind.

We now look at the distribution of several important parameters :- the force on the anchor, the angle of this force to the horizontal, the tension at the top of the mooring and the movement of the top of the mooring in the direction of the force. These are shown in figures 37-40 for the north wind and the south east wind cases and for the northern and southern ends of each net unit.

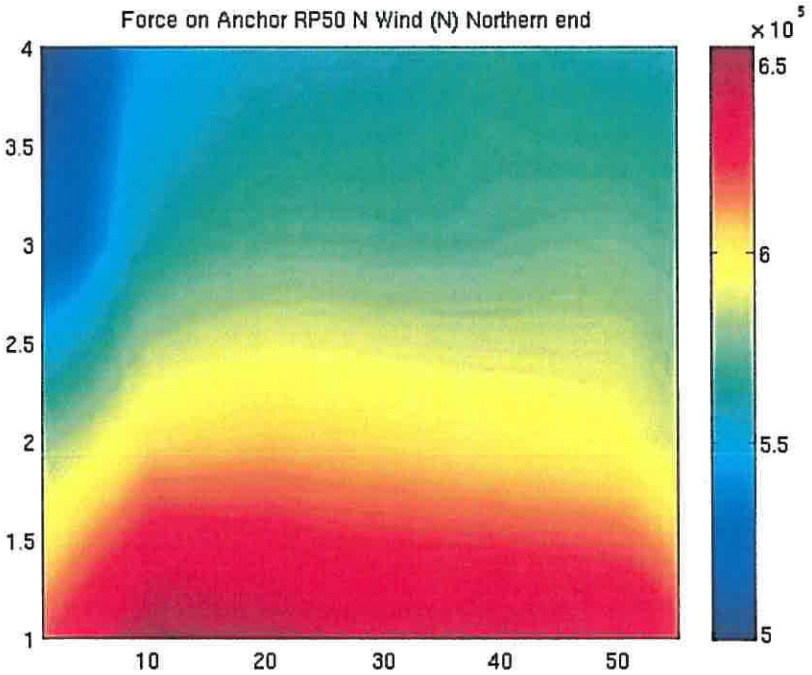

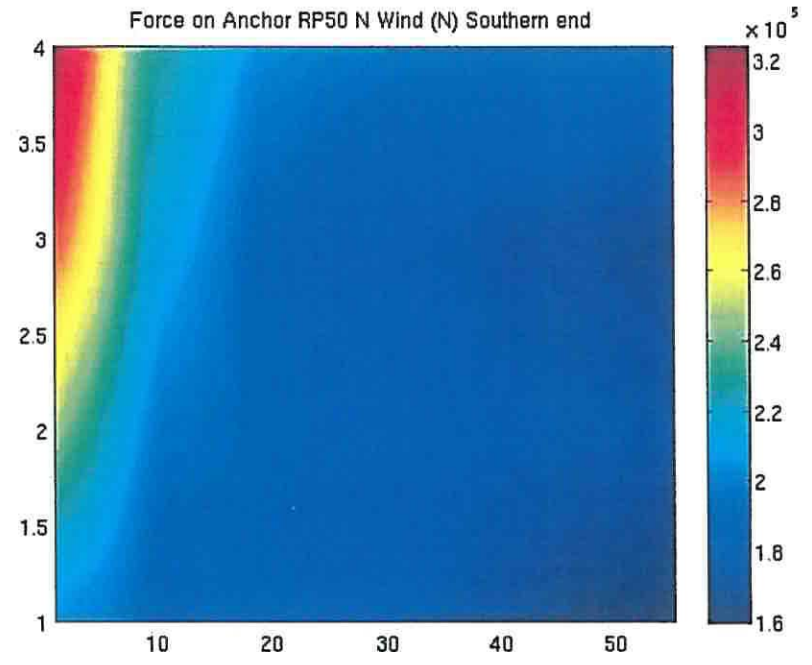

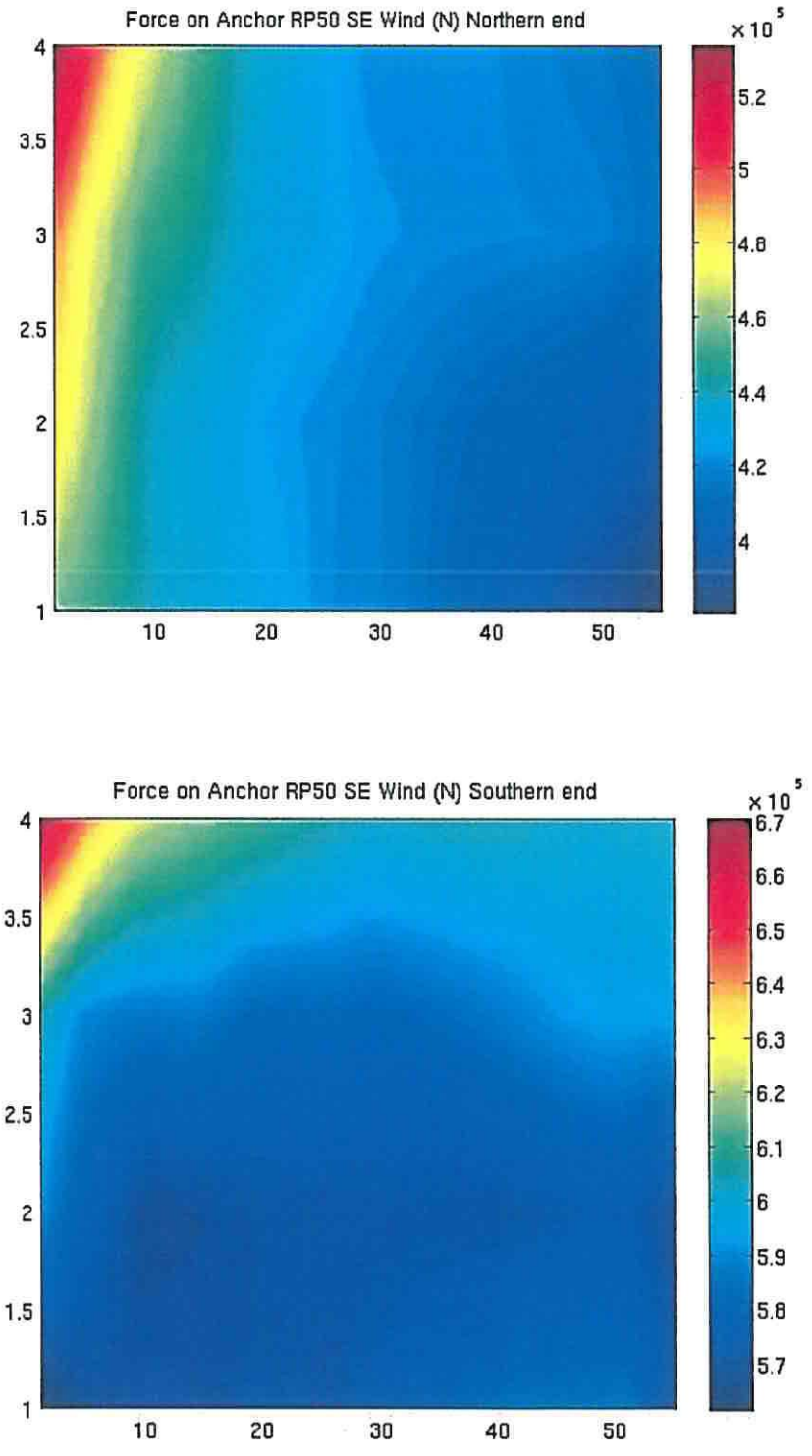

Figure 37. Force at the anchor for the RP50 north and south east wind cases.

Angle of the Chain at the Anchor to the Horizontal RP50 N Wind (Deg.) Northern end

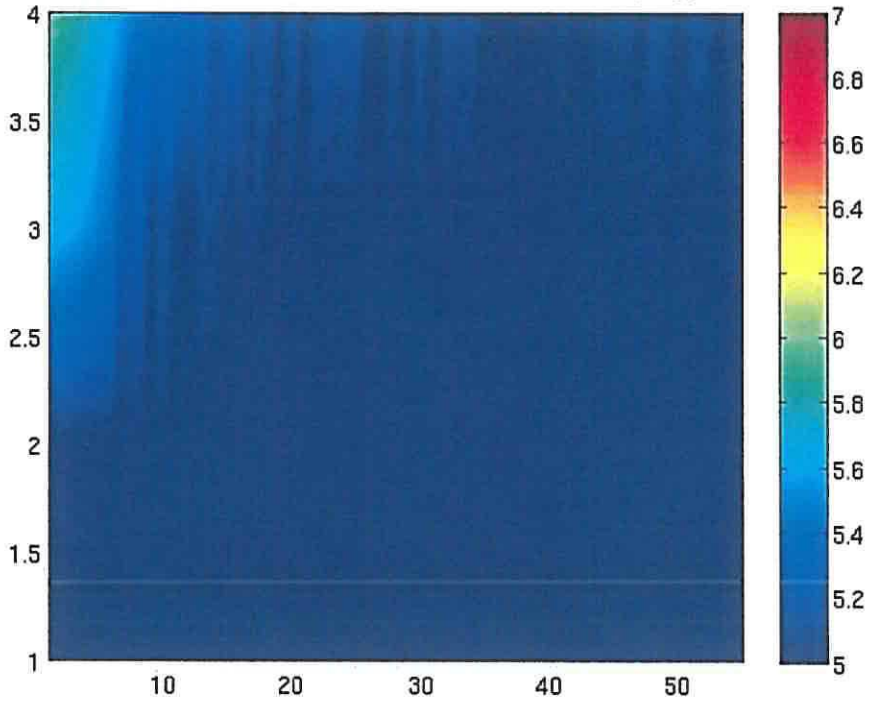

Angle of the Chain at the Anchor to the Horizontal RP50 N Wind (Deg.) Southern end

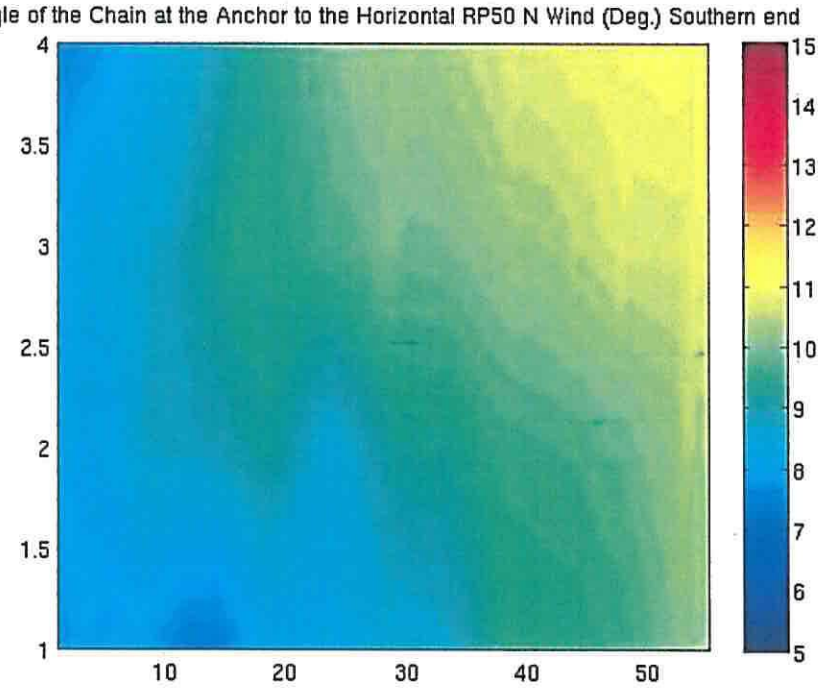

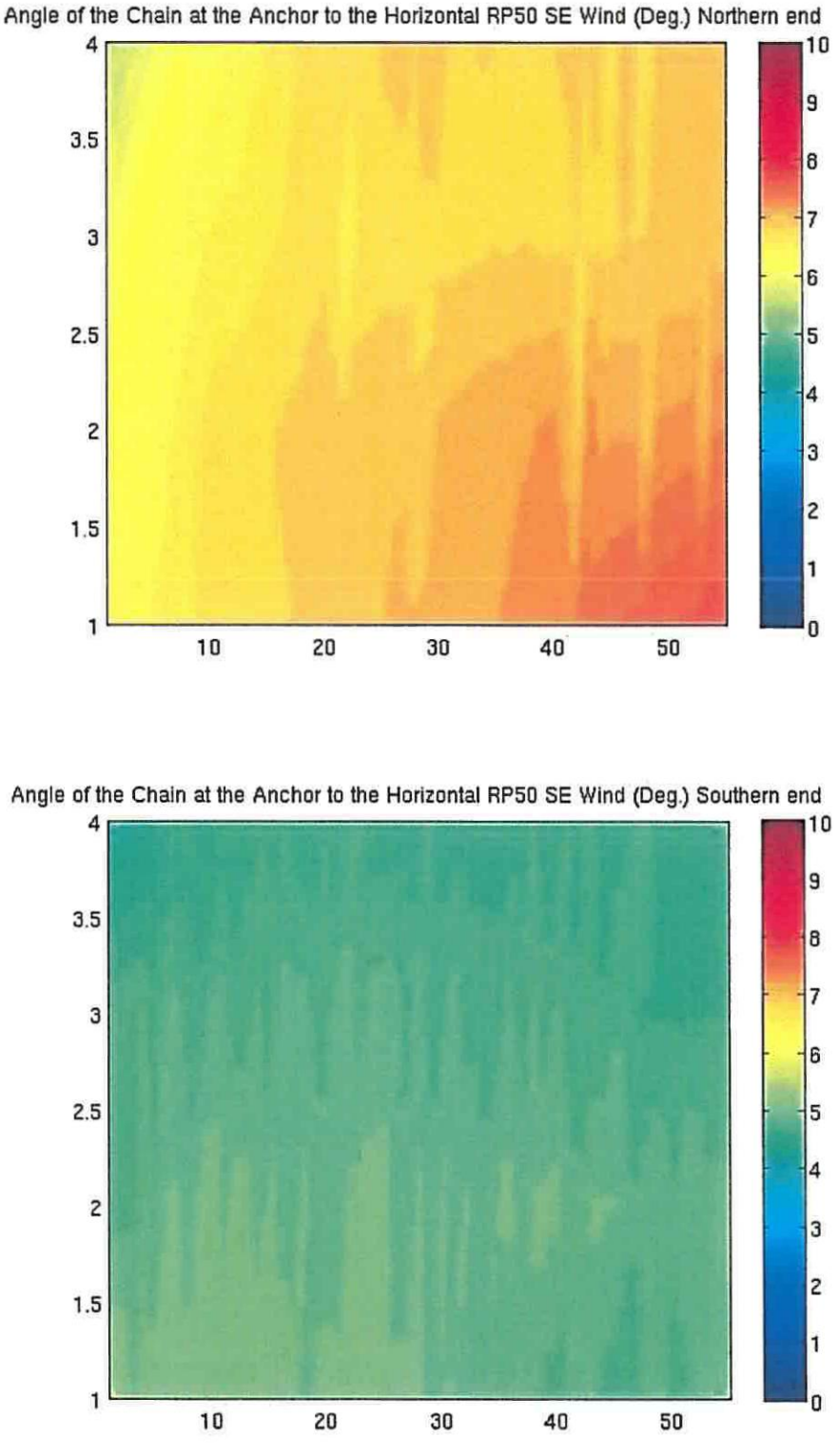

Figure 38. Angle of the chain at the anchor to the horizontal for the RP50 north and south east wind cases.

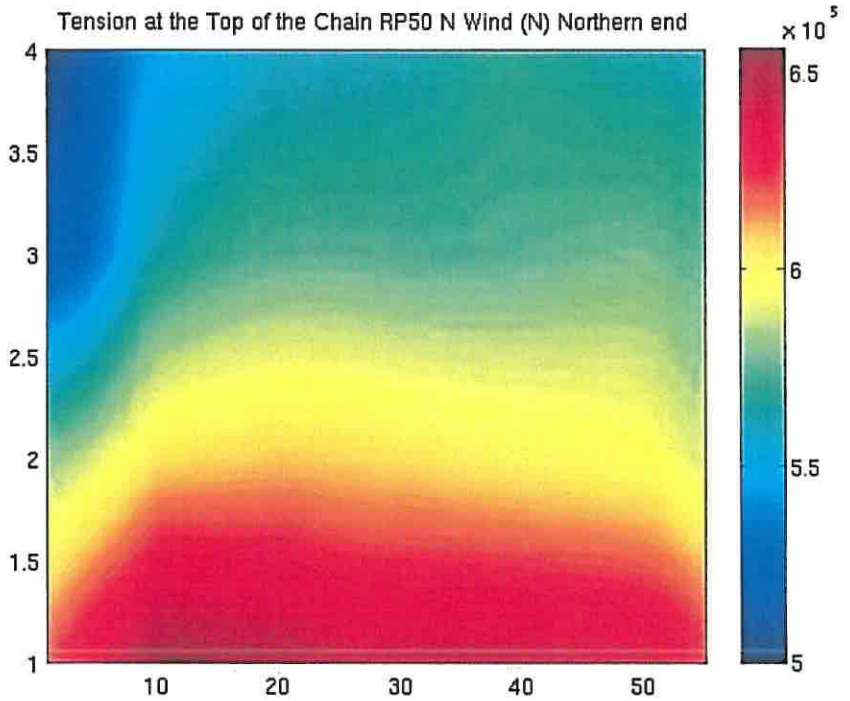
Tension at the Top of the Chain RP50 N Wind (N) Northern end
x 10^5
6.5
6
5.5
5
4
3.5
3
2.5
2
1.5
1
10
20
30
40
50

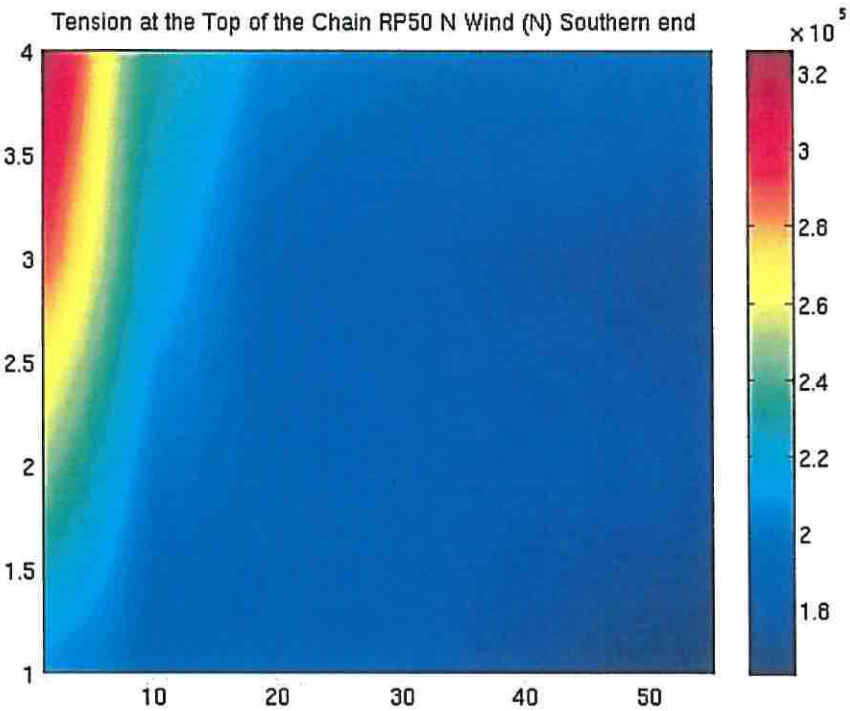
Tension at the Top of the Chain RP50 N Wind (N) Southern end
x 10^5
3.2
3
2.8
2.6
2.4
2.2
2
1.8
4
3.5
3
2.5
2
1.5
1
10
20
30
40
50

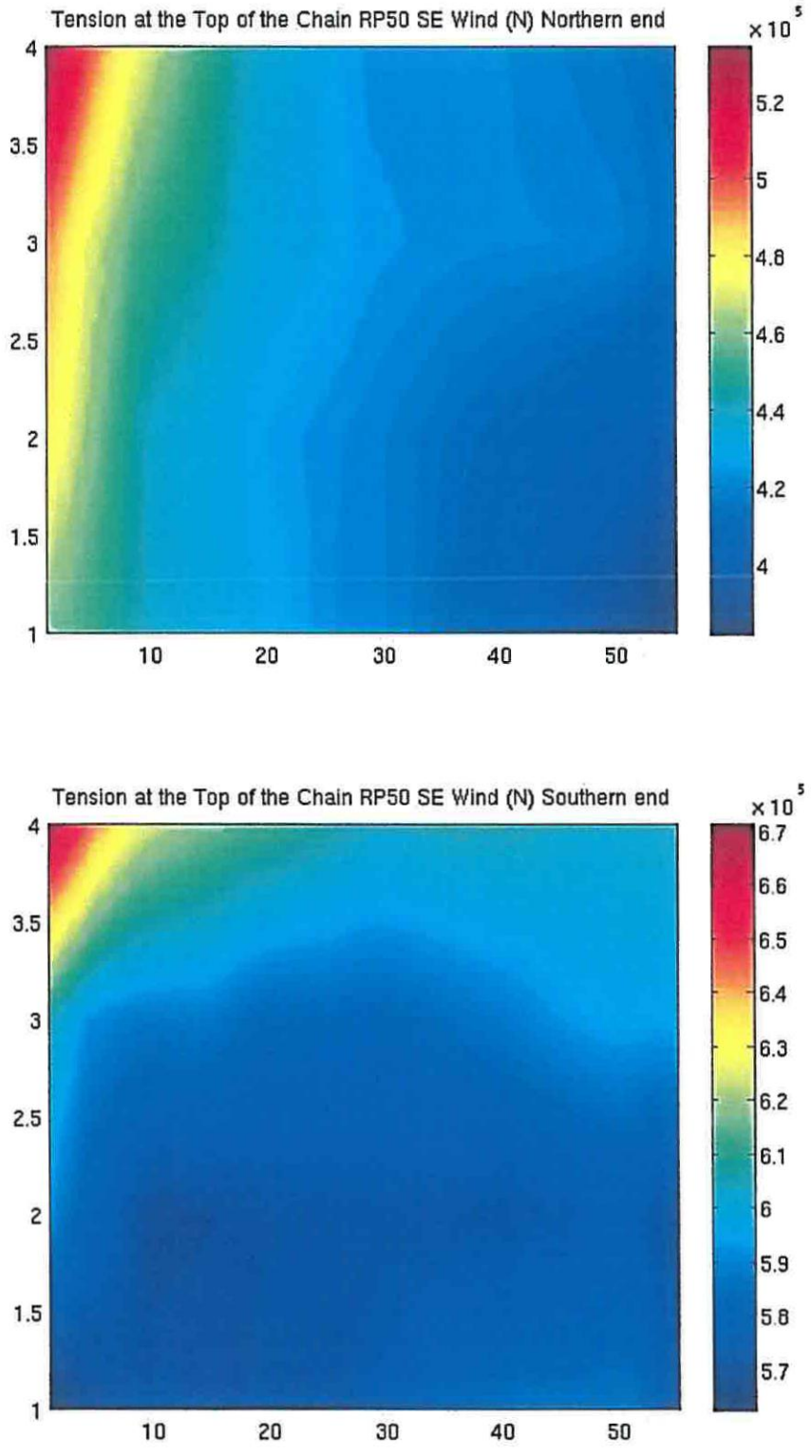

Figure 39. Tension at the top of the mooring chain for the RP50 north and south east wind cases.

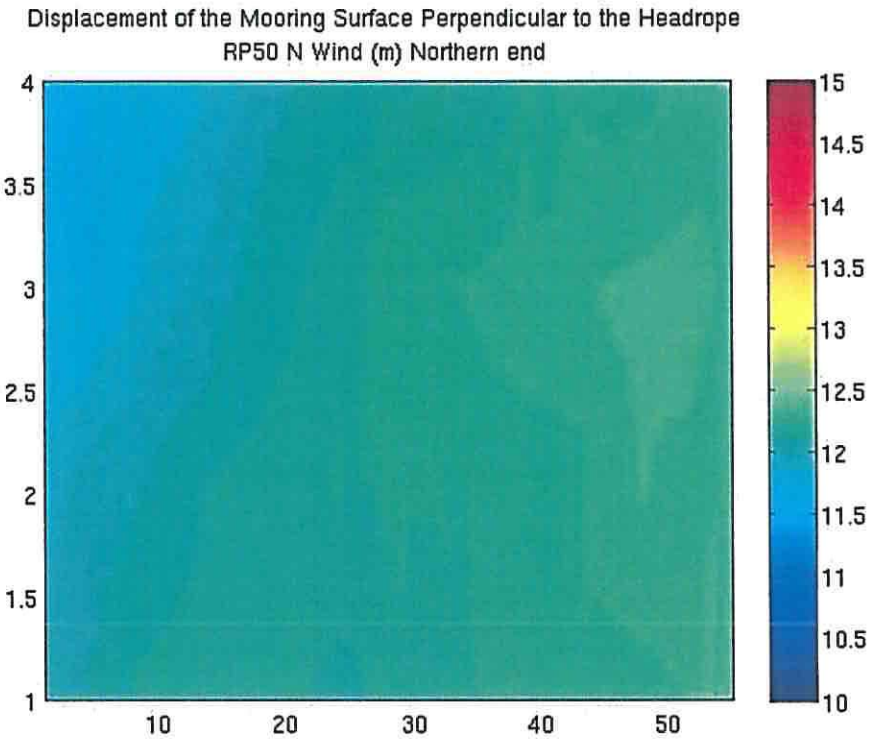
Displacement of the Mooring Surface Perpendicular to the Headrope
RP50 N Wind (m) Northern end
4
3.5
3
2.5
2
1.5
1
10
20
30
40
50
15
14.5
14
13.5
13
12.5
12
11.5
11
10.5
10

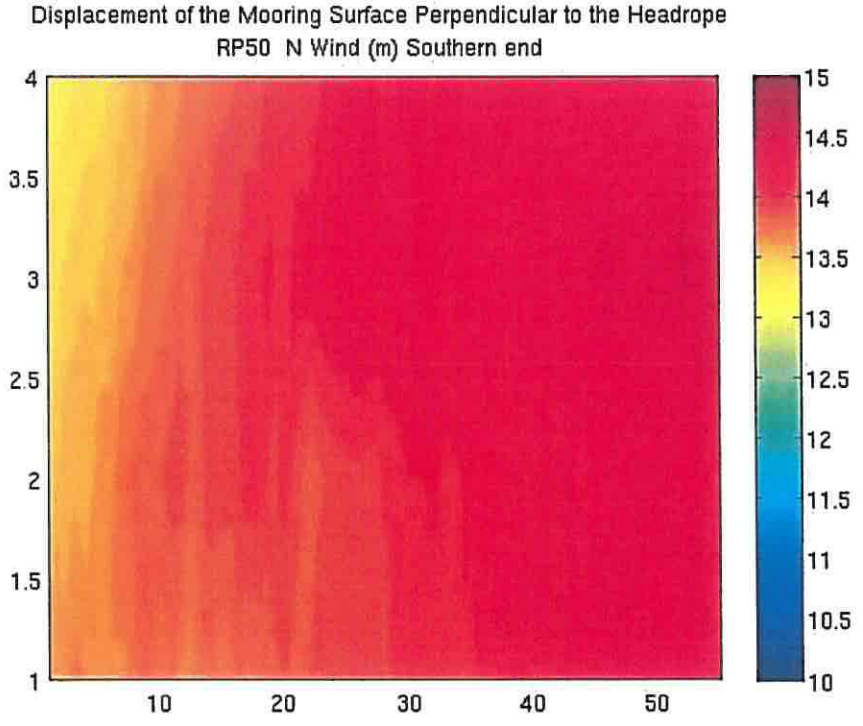
Displacement of the Mooring Surface Perpendicular to the Headrope
RP50 N Wind (m) Southern end
4
3.5
3
2.5
2
1.5
1
10
20
30
40
50
15
14.5
14
13.5
13
12.5
12
11.5
11
10.5
10

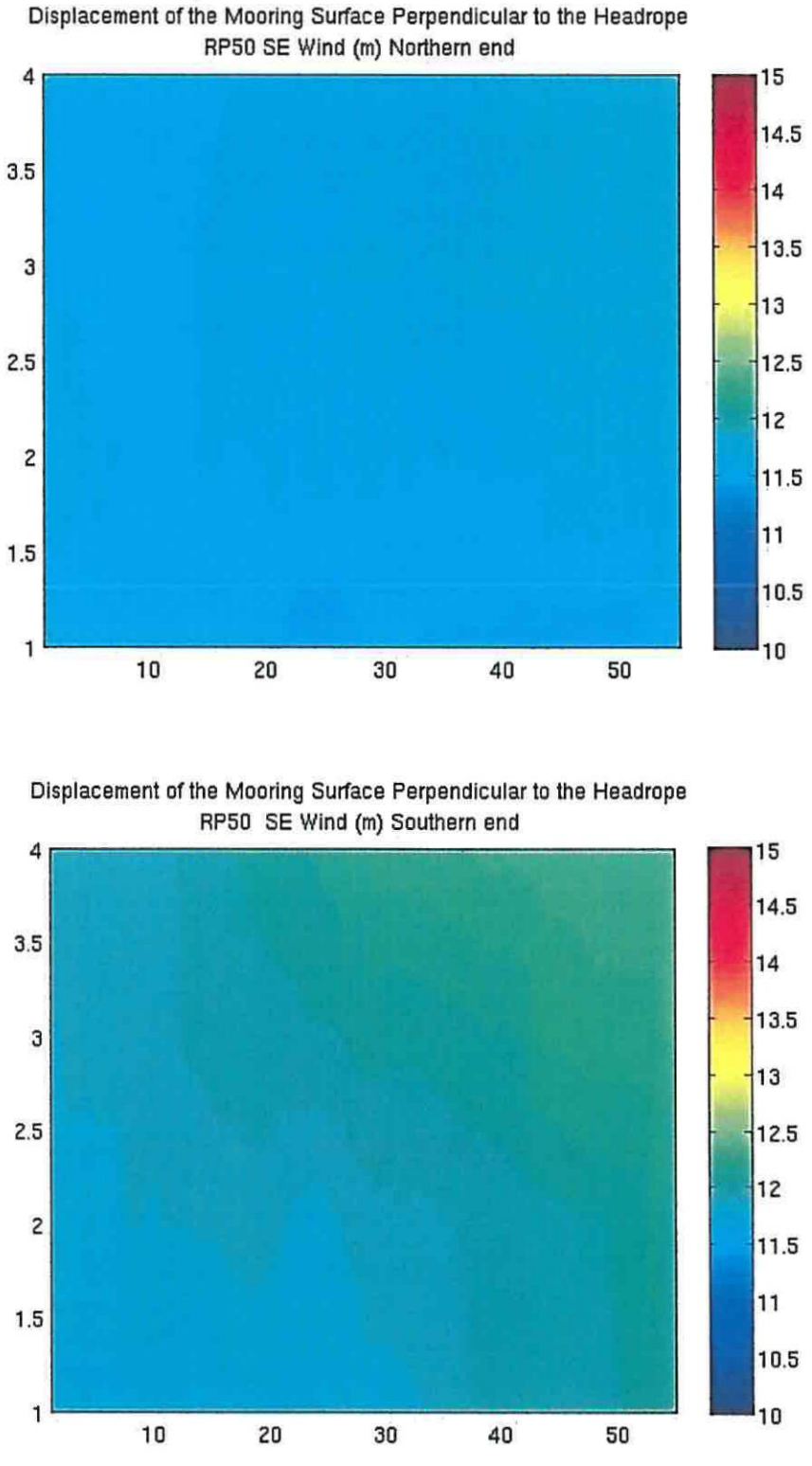

Figure 40. Displacement of the surface of the mooring in the direction perpendicular to the headrope for the RP50 north and south east wind cases.

The maximum force on the anchor for all RP50 wind forcing cases occured at x=1, y=55 for the south east wind and was 670.4 kN (68.3 tonnes force). The forces for the north wind were very slightly lower than these values, but this time occurred along the southern row of net units.

The angle to the horizontal of the chain under load did not exceed 11.1 degrees.

The maximum tension at the top of the anchor chain was 671.3 kN (68.4 tonnes force), occurring under the south east wind condition. This compares with the breaking load of the anchor chain of 115.3 tonnes force.

The displacement of the upper end of the moorings was greatest where there was the most depth (NE corner). It was always lower than 14.4 m, compared to the net unit spacing of 10.0 m. All the headropes should displace approximately 15 m at their centres. The relative displacement of the nets (i.e. the difference between adjacent net units) will be less than this, so we do not expect the net units to touch each other under extreme RP50 forcing.

This report is accompanied by a spreadsheet with exact locations of each anchor, the values of anchor force, the tension at the top of the chain and the displacement of the top of the mooring for each of the wind directions N, NE, E, SE and S.

9.0 Conclusions and Recommendations

A methodology has been developed to calculate the force at the end of the mooring caused by a combination of the 50 year Return Period extreme wind and spring tide on a flexible net structure. A layout for the net units has been proposed where they are separated by 10 m. This allows a configuration of 55 x 4 units in the proposed license area, allowing for a 30 m margin to the east and the west of the nets. This is the layout that has been tested.

The tension in each net has been calculated and it has been shown that even allowing for the deformation of the headropes and the shape adopted by the moorings, the headropes will not touch each other under the extreme forcing conditions for any wind direction. From this layout, individual net units can be removed for access by larger vessels.

The total velocity of the combined current from transient currents from waves, the theoretically maximum tide, wave Stokes drift and surface wind stress experienced by the nets have been calculated as varying spatial fields. It was found that the wave orbital motion is nearly an order of magnitude bigger than the other currents.

The extreme instantaneous currents cause a tension in the headrope that is calculated to be within the sensible conditions for the 90 mm Polypropylene multibraid headrope. This is because the headropes are allowed to deform considerably (15 m) in response to the currents and this has been taken into consideration in the calculations made here.

Under the extreme instantaneous currents, the nets are calculated to lift like a curtain and will almost become horizontal for both the juvenile mussel laden nets and for the situation pre-harvest with the the maximum mussel loading. Both conditions are similar, since in the juvenile case, the mussels do not create much drag (low solidity factor) and for the pre-harvest case, the extra drag is offset by the weight of the mussels.

The forces experienced by the nets were similar when the wind was from either the north, north east, east or south east. This was due to both the fetch of the wave generation and the protection offered by nearby sand banks. For winds from the south, the site is protected by a sand bank. For south and south west winds, only long period swell waves generated in the Atlantic propagate into the area.

By using screw anchors instead of more conventional anchors, it has been possible to design a compact net unit layout. The mooring scope was set to 60 m, so that there was a nearly taut mooring chain in response to the extreme forces leading to a vertical force on the anchor chain, but this should be well within the limits of the pullout force in the coarse sand substrate to be found in the area. By using a 60 m mooring scope, the adjacent net units do not touch each other in any circumstance, therby justifying the chosen 10 m spacing of the units. The tensile strength of the anchor chain used was not exceeded.

9.0 References

Waves in Oceanic and Coastal Waters by Leo H. Holthuijsen 2007

Løland, G. (1991). Current Force On and Flow Through Fish Farms. Ph.D. thesis, The Norwegian Institute of Technology.

H. M. Irvine and G. B. Sinclair, THE SUSPENDED ELASTIC CABLE UNDER THE ACTION OF CONCENTRATED VERTICAL LOADS. Int. J. Solid Structures, 1976, Vol 12 pp. 309-317. Pergamon Press.

S. Weller, Davies, P., Lohanning, L., and Banfield, S. (2013) Guidance on the use of synthetic fibre ropes for marine energy devices. Merific Project, Ifremer reference: RDT CSM 13-232

END